Title: Single-cell Landscape Analysis of the Human Circulating B Cell Pool under Selective Pressure of Allogeneic Stem Cell Transplantation

Authors: Jonathan C. Poe[1†], Jiyuan Fang[2†], Dadong Zhang[3†], Marissa R. Lee[2], Rachel A. DiCioccio[1], Hsuan Su[1], Xiaodi Qin[3], Jennifer Zhang[4], Jonathan Visentin[1,5,6], Sonali J. Bracken[7], Vincent T. Ho[8], Kathy S. Wang[8], Jeremy J. Rose[9], Steven Z. Pavletic[9], Frances T. Hakim[9], Wei Jia[1], Amy N. Suthers[1], Itaevia Curry-Chisolm[1], Mitchell E. Horwitz[1,3], David A. Rizzieri[1,3], William McManigle[1], Nelson J. Chao[1,3,10], Adela R. Cardones[4], Jichun Xie[2,3], Kouros Owzar[2,3], and Stefanie Sarantopoulos[1,3,10]*

Affiliations:

[1]Department of Medicine, Division of Hematological Malignancies and Cellular Therapy, Duke University Medical Center; Durham, NC, USA.

[2]Department of Biostatistics and Bioinformatics, Duke University Medical Center; Durham, NC, USA.

[3]Duke Cancer Institute, Duke University Medical Center; Durham, NC, USA.

[4]Department of Dermatology, Duke University Medical Center; Durham, NC, USA.

[5]Department of Immunology and Immunogenetics, Bordeaux University Hospital; Bordeaux, France.

[6]UMR CNRS 5164 ImmunoConcEpT, Bordeaux University; Bordeaux, France.

[7]Department of Medicine, Division of Rheumatology and Immunology, Duke University Medical Center; Durham, NC, USA.

[8]Division of Hematologic Malignancies and Department of Medical Oncology, Dana-Farber Cancer Institute; Boston, MA, USA.

[9]Experimental Transplantation and Immunology Branch, National Cancer Institute; Bethesda, MD, USA.

[10]Department of Immunology, Duke University Medical Center; Durham, NC, USA.

*Corresponding author. Email: stefanie.sarantopoulos@duke.edu

[†]Equal contribution to this work

ABSTRACT

A healthy immune state is achieved and maintained only if autoreactive B cells are eliminated or tolerized. B cells play a substantiated role in the pathobiology of the allogeneic hematopoietic stem cell transplantation (allo-HCT)-related autoimmune-like syndrome, chronic graft versus host disease (cGVHD). After allo-HCT, donor-derived B cells continually develop under selective pressure from host alloantigens and known to be B Cell Receptor (BCR)-activated in cGVHD. Thus, allo-HCT represents a unique opportunity to study human peripheral B cell tolerance. We performed scRNA-Seq analysis on high numbers of purified B cells from allo-HCT patients. Our unsupervised analysis revealed 10 clusters, distinguishable by signature genes for maturation, activation and memory. Compared to scRNA-Seq data from healthy or infected individuals, allo-HCT patients had striking transcriptional differences in the 'memory' B cell compartment that suggested a propensity toward autoreactivity. To identify B-cell intrinsic properties linked to overt loss of immune tolerance in allo-HCT, we then assessed clusters for differentially expressed genes (DEGs) between patients with vs. without autoimmune-like manifestations (Active cGVHD vs. No cGVHD, respectively). In Active cGVHD, we found notable DEGs in both naïve and BCR-activated clusters, including a BCR-experienced 'memory' cluster with a significantly expanded atypical/age-related memory B cells (ABCs) population. Pseudotime trajectory analyses of B-cells before and after in vitro exposure to a 'maturation' agent indicated that aberrant B-cell activation and diversification states after allo-HCT are potentially 'plastic.' Our single-cell-level findings reveal potentially novel therapeutic targets in cGVHD and provide new understanding of how alloreactivity may lead to human autoimmune diseases.

One Sentence Summary:

Our scRNA-Seq study of purified B cells after allo-HCT clarifies human B cell subsets and molecular differences when immune tolerance is lost or maintained.

Main Text:

INTRODUCTION

Operational B cell tolerance checkpoints normally function to silence the high proportion of potentially self-reactive peripheral B cells that recirculate and can mediate immune pathology (*1*). In the condition termed chronic graft-versus-host disease (cGVHD), a syndrome acquired by some, but not all patients undergoing allogeneic hematopoietic stem cell transplantation (allo-HCT), B cells have a substantial role (*2, 3*). Aberrant peripheral B cell activation, survival, and maturation signaling pathways are thus promising therapeutic targets for cGVHD patients (*4*). Regulatory B cells (Breg) also appear to be important in controlling the severity of cGVHD in both humans and mice (*5, 6*). B cell recovery and homeostasis after allo-HCT are both altered in cGVHD, whereby extrinsic factors including BAFF (B cell-activating factor belonging to the tumor necrosis factor [TNF] family) contribute to a break in B cell tolerance (*7-12*).

B cells continually regenerate. After allo-HCT, B cells from donor stem cells and progenitor cells that are major histocompatibility antigen (HLA)-matched or mismatched replace the recipient (host) immune system. Prior to allo-HCT, high dose chemotherapy and/or radiation conditioning creates "space" in the B cell compartment whereby excess BAFF promotes antigen-activated B cells (*11*). In a mouse model, alloantigen and BAFF operate together to promote the loss of B cell tolerance that occurs in cGVHD (*8*). BAFF is also known to mediate B-cell driven

autoimmune and fibrotic manifestations akin to findings in cGVHD (*13*). After allo-HCT donor T cells recognize host polymorphic or alloantigens in a coordinated T-B response (*14*), and follicular helper T cells are required for B cell anti-host reactivity and cGVHD development (*15*). The peripheral B cell compartment in patients with active disease (Active cGVHD) becomes enriched for B-cell receptor (BCR)-stimulated and IgG-secreting populations (*2, 3, 7, 9, 16-19*). Despite these advances, how constant exposure to alloantigens and high BAFF alter intrinsic B cell pathways in human allo-HCT remains unknown.

Compared to allo-HCT patients without autoimmune manifestations (No cGVHD), those with Active cGVHD have a circulating B cell compartment with a propensity toward activation (*10, 20*) and potential 'exhaustion' (*21*), yet intricately defining the pleomorphic outcomes on B cell subset diversity resulting from cGVHD genesis remains elusive. Human allo-HCT and the advent of single-cell RNA-sequencing (scRNA-Seq) now enables identification of potential intrinsic B cell pathways that potentially underpin pathological functions. We utilized scRNA-Seq to delineate transcriptional programs within 10 peripheral B cell clusters resolved in allo-HCT patients. We also identified important differentially expressed genes (DEGs) within these clusters that were associated with Active cGVHD. Some DEGs were spread across these B cell populations, while others were restricted to certain B cell subsets. Homing and cell cycle genes including *GPR183* and *CKS2*, respectively, were overexpressed in circulating transitional, activated and memory subsets, suggesting potential roles in B cell dysfunction from the time B cells first emerge in the periphery, and then after alloantigen BCR stimulation. Within the 'memory' cluster, potentially-pathogenic 'atypical/age-related' B cell (ABC) populations found in both health and autoimmune disease (*22, 23*) were expanded in Active cGVHD, and drivers of ABCs including *TBX21* (*TBET)* and *ZEB2* (*22, 24, 25*) were increased DEGs. We further

confirmed significant expansion of ABC subsets in Active cGVHD using high-dimensional flow cytometry analysis. Finally, comparison of our allo-HCT scRNA-Seq data with a publically-available dataset on blood B cells from healthy donors (HDs) and non-HCT patient groups highlighted distinct signature gene profiles within both ABC and typical memory subsets unique to the allo-HCT setting. Thus, our study provides new insight into the diversity of the peripheral B cell compartment after allo-HCT, and identifies potential molecular targets for future study that may effectively alleviate cGVHD and other B cell-mediated autoimmune diseases.

RESULTS

The circulating B cell compartment arising after allo-HCT comprises transitional, naïve, antigen-stimulated, and memory single-cell signature gene profiles

To assess molecular features of human B cells that regenerate and circulate in an alloantigen-rich environment when immune tolerance has been achieved or lost, we analyzed highly purified viable B cell samples (**Fig. 1A**) from 8 patients >10 months (mos) post allo-HCT. Four patients had Active cGVHD (median = 12.6 mos post-HCT) and 4 patients had no clinical history of cGVHD (No cGVHD, median = 11.5 mos post-HCT), **table S1**. Unsupervised clustering analysis of the 8-patient scRNA-Seq dataset identified 10 clusters of B cells (**Fig. 1B**). To confirm cell types, inferences were made by examining the relative expression of genes representing B cells (*PAX5*, *CD22*), and rare residual T cells (*CD3E*) and monocytes (*LYZ*) (**fig. S1**). All 10 B cell clusters were represented in both Active and No cGVHD patient groups (**Fig. 1C**). We numbered these clusters 1-10 from largest to smallest total number of cells in both patient groups combined. (**Fig. 1D**).

To validate known and potentially novel B cell subsets in allo-HCT patients, we first identified hallmark 'signature' (marker) genes to distinguish each B cell cluster. We then plotted the log2 normalized expression values for 16 major B cell development and function genes from all 8 transplant samples (**Fig. 1, E-H**), all validated using 'findMarkers' in the R package Seurat (*26*). Within clusters, all signature genes assessed were remarkably homogeneous among all 8 allo-HCT patients. Levels of the transitional B cell molecules *VPREB3*, *CD24* and *IRF8* were highest in Clusters 1 and 2 (**Fig. 1E**), with Cluster 1 primarily expressing kappa Ig light chain and Cluster 2 primarily expressing lambda Ig light chain (*IGKC* and *IGLC3*, respectively, **Fig. 1F**). High expression of *LTB* further supports that B cell Clusters 1 and 2 represent recent bone marrow (BM) emigrants because lymphotoxin beta is required for follicle development in the spleen (*27*) and expressed highest in late transitional B cells (immgen.org). Clusters 1, 2 and 3 expressed the highest levels of the IgM heavy chain gene (*IGHM*). Cluster 3 likewise showed high *IGKC* expression and intermediate *IGLC3* expression (**Fig. 1F**). Unlike Clusters 1 and 2, Cluster 3 had lower expression of *CD24* and *IRF8*, and higher *IRF4*, suggesting a more mature B cell stage. Clusters 9 and 10 expressed similarly high levels of microRNA-155 (*MIR155HG*, **Fig. 1G**), essential for B cell antibody isotype switching (*28*). Clusters 9 and 10 also showed similarly high expression of both *MYC* and *NFKB1* transcripts, suggesting these B cells may be poised to enter the cell cycle. Cluster 10 had uniquely high levels of the chemokine *CCL22*, indicating that Cluster 10 may harbor B cells poised to interact with T-follicular helper cells within the secondary lymphoid organ (SLO) microenvironment. By contrast, Cluster 5 expressed high levels of *CD27*, along with Ig heavy chain genes for IgG1 and IgG3 (*IGHG1* and *IGHG3*, respectively), indicating an enrichment for isotype-switched memory B cells (**Fig. 1H**). Cluster 5 also expressed the highest *ITGAX* (*CD11C*), a distinguishing marker of ABCs found in normal individuals and expanded

during infections and in some autoimmune diseases (*29, 30*). In **Fig 1I**, we depict 3-dimensional (3-D) UMAP plots to further highlight the spatial relationships among neighboring B cell clusters.

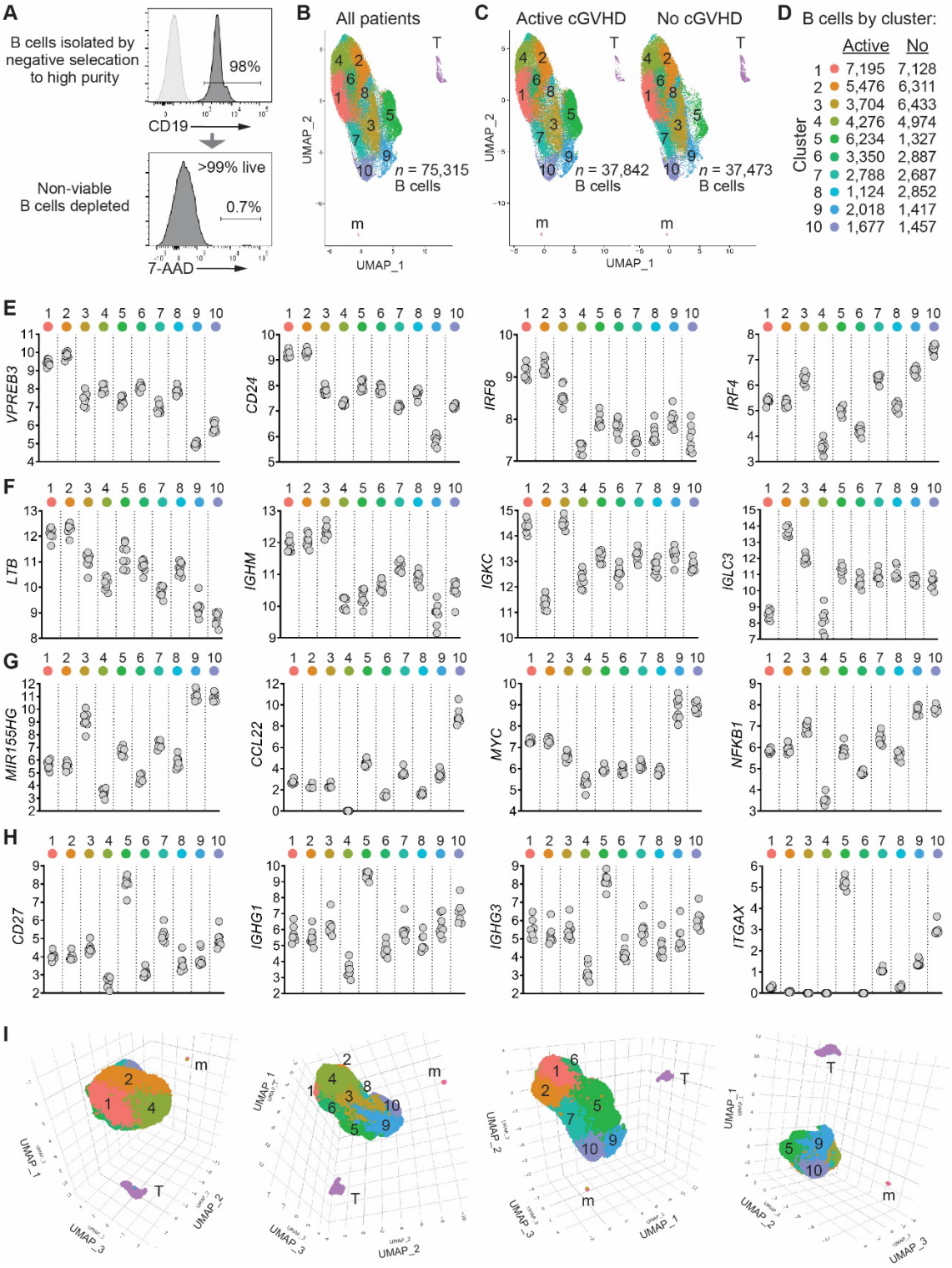

Fig. 1. Unsupervised clustering analysis of scRNA-Seq data reveals multiple B cell subsets characterized by signature genes in allo-HCT patients. (**A**) Representative flow cytometry histograms showing B cell purity and viability among PBMCs from an allo-HCT patient. 10,000

high-quality B cells per patient sample isolated in the same manner were targeted for 10X Genomics single-cell library construction (*n*=4 No cGVHD, *n*=4 Active cGVHD). (**B**) Two-dimensional (2D) Uniform Manifold Approximation and Projection (UMAP) expression profiles of all untreated cells from the 8 allo-HCT patients. Numbers indicate each of the 10 major clusters identified as B cells, which were distinct spatially from the small clusters of residual cells identified as T cells (T) and monocytes (m). Total high-quality B cells in the analysis are indicated. (**C**) UMAP as in panel (B), with B cells partitioned by allo-HCT patient group. Total high-quality B cells per group are indicated. (**D**) Number of B cells mapping to each of the 10 B cell clusters by patient group. **(E-H)**, Log2 normalized expression of genes indicative of B cell maturity (E, F), along with activation, antibody production potential, and memory markers (G, H), by B cell cluster. Each symbol (gray circle) represents regularized log-transformed gene counts (*31*) [y-axes] from one of the 8 allo-HCT patients. **I**, Three-dimensional (3D) UMAP projections of B cells from all patients [as in (B)], viewed at different angles of rotation.

Allo-HCT B cell clusters can be delineated by signature genes involved in different B cell pathways

Based on the signature gene results in **Fig. 1E-I**, along with data presented in **Fig. 2**, we reordered the 10 B cell clusters empirically according to maturation, activation and memory status. We started with the least mature/activated first, based on general knowledge about B cells as they enter the periphery and eventually encounter antigen/co-stimulatory signals. The following cluster order was thus used from **Fig. 2** onward: Cluster 1, 2, 4, 6, 8, 7, 3, 9, 10 and 5. In **Fig. 2A,C-H** colored squares in the heat maps indicate signature genes of interest (rows) reaching significance (P_{adj} <0.05) in the B cell cluster indicated (columns), as weighted against all other clusters. Red hues indicate signature gene expression increase, and blue hues indicate signature gene expression decrease, (log FC expression level, indicated by scales). Notably, Clusters 1, 2, 4, 6 and 8 retained one or more hallmark genes of B cell immaturity, while Clusters 7, 3, 9, 10 and 5 expressed markers of antigen activation, cytoskeletal activity, or the capacity to produce antibodies (**Fig. 2A,B**). This ordering of the 10 B cell clusters was further validated by interrogating the Kyoto Encyclopedia of Genes and Genomes [KEGG] (*32*) and Gene Ontology [GO] (*33*) databases using signature genes of interest. We then grouped these signature genes into major molecular pathways (**Fig. 2C-H** heat maps). Clusters 9 and 10 showed high expression of genes involved in B cell–T cell interactions, transcription, proliferation, survival, and metabolic processes (**Fig. 2A,C-H**), correlating with high relative expression of *MYC* and *NFKB1* (**Fig. 1G**). Clusters 7 and 10 shared increases in multiple ribosomal genes (**Fig. 2G**), suggesting relatedness for protein synthesis potential. Overall, clusters 6 and 8 had relatively fewer gene level increases, suggesting relative quiescence, although Cluster 6 had strong expression of actin cytoskeleton organizer *CDC42SE1* and the proto-oncogene *MENT* (previously *C1orf56,* **Fig. 2F**). Interestingly, the less mature/less

activated subsets (Clusters 1, 2, 4 and 6) trended toward more decreased signature genes ('Down', **Fig. 2I**), while the activated/memory subsets (Clusters 3, 9, 10 and 5) trended toward more increased signature genes ('Up', **Fig. 2I**). Our data thus uniquely elucidate a hierarchy and relatedness among peripheral B cell clusters arising in human allo-HCT.

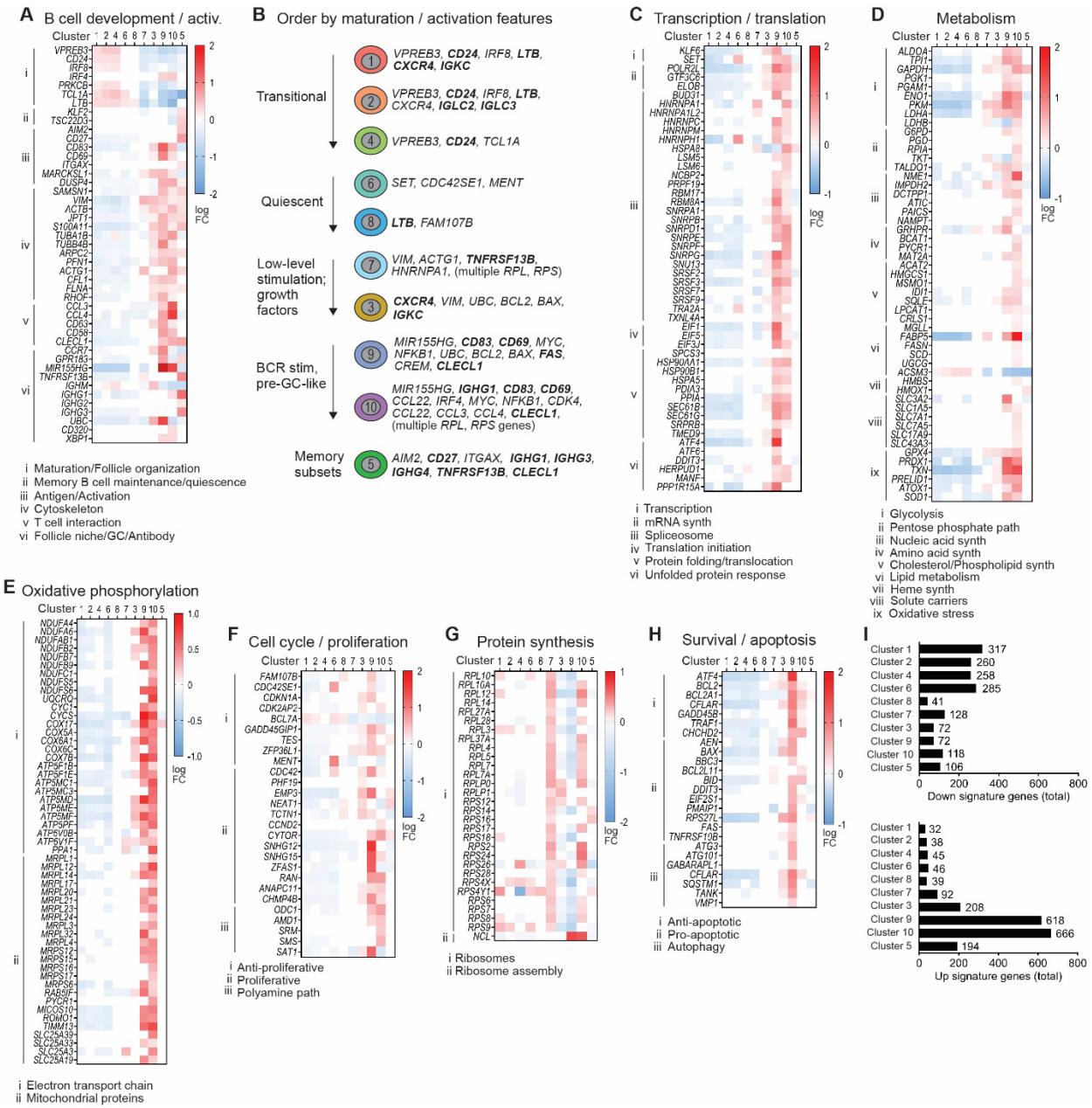

Fig. 2. Signature genes manually assigned to biological pathways further highlight allo-HCT B cell cluster inter-relatedness and features of B cell development and activation. (**A**) Signature (marker) genes related to B cell development and activation, assessed in an inter-cluster of all 8 allo-HCT patients in the scRNA-Seq data set by manually interrogating the KEGG and GO databases. Each colored square represents a significant (P_{adj} <0.05) log fold change (log FC) value for the gene indicated (rows), in the B cell cluster indicated (columns). Red shading indicates

increased signature gene expression, while blue shading indicates decreased signature gene expression, as weighted against all other clusters. Clusters were ordered empirically from the least differentiated (Cluster 1, Igκ$^+$ transitional) to most differentiated (Cluster 5, memory) as described in the Results section. Genes were further subdivided to one of the specific pathways indicated by the roman numerals at left and corresponding key below. (**B**), Cartoon depiction of B cell clusters and their associated signature genes that further categorize these subsets (as labeled at left). Signature genes encoding surface proteins are highlighted in bold font. (**C-H**) As performed in (A), signature genes were assessed in the major biological pathways indicated above each heat map, and subdivided by the more specific pathways indicated by the roman numerals at left and corresponding keys below. (**I**) Total numbers of signature genes reaching significance within each cluster, being either decreased ('Down signature genes', top graph) or increased ('Up signature genes', bottom graph).

BCR-experienced 'memory' Cluster 5 includes an extrafollicular-like ABC population expanded in Active cGVHD

Antigen-experienced 'memory' B cells likely include pathogenic B cells that emerge in cGVHD, as occurs in other diseases such as lupus (*1, 34*). We thus further interrogated CD27-expressing 'memory' Cluster 5. In addition to a CD27-expressing population, Cluster 5 also harbored B cells expressing *ITGAX* that encodes CD11c, which broadly marks ABC populations that also lack CD21 ($CD11c^{+}CD21^{-}$). ABCs have a pathogenic role in both autoimmunity and chronic inflammation, revealing a functional complexity of these 'memory' B cells (*29, 35, 36*). ABCs are often termed either 'atypical' or 'age-related' B cells, the latter term originally given because ABCs accumulate in aged mice (*37, 38*). ABCs are considered 'atypical' because they undergo activation and differentiation outside of the germinal center (GC), rapidly homing to the outer follicle as 'extrafollicular' B cells (*39, 40, 41*). To elucidate 'memory' subpopulations in cGVHD, we examined the pattern of *CD27* and *ITGAX* expression in Cluster 5. As shown in **Fig. 3A,** B cells expressing either *CD27* (left UMAPs) or *ITGAX* (right UMAPs) were largely spatially segregated within Cluster 5, suggesting largely independent subsets. To validate this finding, we performed flow cytometry analysis on blood B cells from an independent cohort of allo-HCT patients. As shown in **Fig. 3B**, allo-HCT B cell subsets primarily expressed either CD27 or CD11c alone, with a smaller subset expressing both markers (double-positive, 'DP'). Importantly, $CD11c^{+}CD27^{-}$ ABCs were significantly expanded in Active cGVHD patients compared to No cGVHD patients and HDs [**Fig. 3B,C**]. Interestingly, the $CD11c^{+}CD27^{+}$ 'DP' subset was proportionally lower in the allo-HCT environment compared to HDs (**Fig. 3B,C**). Overall these data are consistent with previous work showing that some $CD11c^{+}CD27^{-}$ ABC subsets are expanded in cGVHD and other diseases, sometimes exhibiting an 'exhausted' phenotype and

refractory to specific external stimuli (*21, 42-44*). To gain further insight, we also examined a subset of CD11c^{+}CD21^{-} ABCs that lacks both CD27 and IgD expression (CD11c^{+}CD21^{-}CD27^{-} IgD^{-}), called 'DN2', that is prevalent in lupus and can produce disease-associated antibodies (*41, 45, 46*). The emergence of ABCs (including DN2) with pathogenic roles is driven by one or more costimulatory signals that cooperate with BCR stimulation (*41, 47*). We found DN2 ABCs were markedly expanded in the blood of Active cGVHD patients relative to No cGVHD patients (**Fig. 3D,E**). These data affirm our scRNA-seq data and advance previous work (*21, 41, 44-46*) suggesting that potentially pathologic ABC subsets arise under constant alloantigen exposure.

To assess B cell surface phenotypes more broadly in allo-HCT and potentially elucidate subsets responsive to excess BAFF (*11*), we added CD24 and TACI (TNFRSF13B) in the context of CD27, IgD, CD11c, CD21 (**Fig. 3F**). Using high-dimensional flow cytometry [PhenoGraph, (*48, 49*)] we identified discreet B cell populations in an unbiased manner from concatenated allo-HCT samples. PhenoGraph analysis resolved 15 clusters, designated by lower case letters 'a-o' (**Fig. 3G**). CD11c^{+} ABCs were primarily resolved by Cluster 'a' (**fig. S2**), significantly expanded in Active cGVHD (**Fig. 3H,I**). By contrast, four clusters consisting of IgD^{+}CD27^{-} naïve-like B cells (Clusters 'b, c, d and e', **fig. S2**) were decreased in Active cGVHD patients (**Fig. 3H**). ABC Cluster 'a' was also TACI^{+}, with a mix of IgD$^{+/-}$ B cells (**fig. S2**). Six clusters expressed high levels of surface TACI (Clusters 'a, h, j, k, l and n', **Fig. 3J and fig. S2**). Cluster 'n' expressed substantially higher surface TACI in some Active cGVHD patients (**Fig. 3J**, arrow), and mapped adjacent to ABC Cluster 'a' in the PhenoGraph UMAP (**Fig. 3G).** Clusters 'j' and 'k' likewise had elevated TACI in some Active cGVHD patients (**Fig. 3J**, arrows). Accordingly, regions of B cells in the scRNA-Seq data having increased *TNFRSF13B (TACI)* transcripts were readily evident in

Active cGVHD (**Fig. 3K**, UMAP boxed region II). These results support previous observations that BAFF is a driver of B cell hyper-responsiveness and alloantibody production in cGVHD (*8*).

To examine how allo-HCT compares to the non-HCT setting, we performed a PhenoGraph analysis of HD blood B cells. The HD analysis also predicted 15 clusters, but HDs had a greater number of B cell clusters marking with CD27 (**fig. S3**, Clusters 'm,n,o') compared to allo-HCT patients (**fig. S2**, Clusters 'l,o' only). Furthermore, in allo-HCT patients Cluster 'o' represented mostly $CD27^{bright}$ B cells that lacked CD21, CD24, IgD and CD11c expression, suggestive of isotype-switched plasmablasts ("PB", **fig. S2**). These were among the rarest in both allo-HCT groups (**Fig. 3H**), and this cluster was notably absent in HDs (**fig. S3**). These data reveal that $CD27^{+}$ B subsets after allo-HCT are abnormal or lacking, extending previous observations (*42*). The relative reduction in $CD27^{+}$ B cells in allo-HCT with reciprocally-expanded ABCs in Active cGVHD is consistent with PhenoGraph findings recently reported in pediatric patients with CVID and related syndromes (*50*).

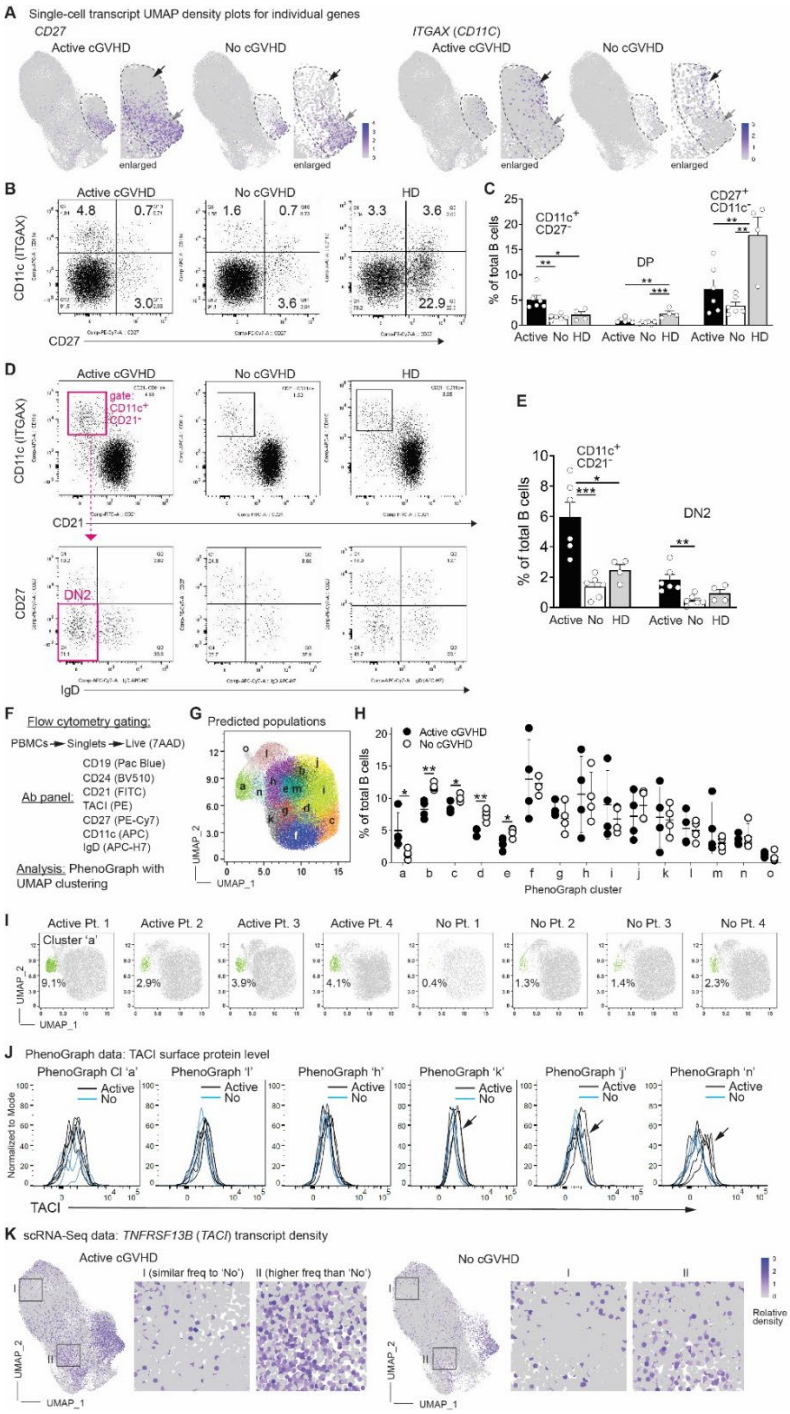

Fig. 3. Cluster 5 contains CD27^{+} 'memory' B cells and ABCs, the latter being expanded in cGVHD. (**A**) B cells expressing *CD27* or *ITGAX* transcripts are enriched in Cluster 5. Shown are UMAP density plots from the scRNA-Seq dataset displaying relative transcript density for the gene indicated, at the single-cell level. The dashed line approximates the perimeter of Cluster 5

(also enlarged for better clarity). Gray arrows indicate a region enriched for *CD27* expressing B cells, and black arrows indicate a region enriched for *ITGAX* expressing B cells. (**B,C**), Flow cytometric analysis to identify ABCs, $CD27^+$ memory B cells, and a small population of $CD11c^+CD27^+$ memory B cells in PBMC samples from a cohort of allo-HCT patients with either Active cGVHD (*n*=6) or No cGVHD (*n*=6), or from HDs (*n*=4). PBMCs were pre-gated on live ($7\text{-}AAD^-$) $CD19^+$ B cells. Dot plots in (B) show representative individuals analyzed from each group. In (C), results from all groups for the $CD11c^+CD27^-$ population, $CD11c^+CD27^+$ (DP) population, and $CD11c^-CD27^+$ population (as gated in (B)) are represented. Statistical comparison was performed using a one-way ANOVA with Tukey's multiple comparisons test (GraphPad Prism 9 software; *, $p<0.05$; **, $p<0.01$; ***, $p<0.001$). (**D,E**), DN2 B cells are expanded in allo-HCT patients with Active cGVHD. (D) Representative FACS plots from PBMCs of allo-HCT patients with Active or No cGVHD, and from a HD, generated after first gating on viable ($7\text{-}AAD^-$), $CD19^+$ B cells, with $CD11c^+CD21^-$ B cells (upper panel gate) and then DN2 B cells ($CD11c^+CD21^-CD27^-IgD^-$) identified in all groups as depicted in magenta for the Active cGVHD sample. (E) Statistical comparison between groups (Active cGVHD, n=6; No cGVHD n=6, HDs, n=4) was performed using a one-way ANOVA with Tukey's multiple comparisons test (GraphPad Prism 9 software; **, $p<0.01$). (**F-J**) Flow cytometry plus PhenoGraph analysis performed on blood B cells from Active cGVHD (*n*=4) or No cGVHD (*n*=4) patients. Shown in (F) is the gating strategy to distinguish B cells (top line), the B cell antibody panel used (middle), and the analysis platform (bottom). Shown in (G) is the concatenated PhenoGraph UMAP plot from all 8 patients, with 15 clusters identified (letters). The graph in (H) indicates B cell frequency within each of the 15 clusters by patient group. Each symbol represents results from one of the 8 patients assessed. Statistical comparisons were performed using a two-tailed, unpaired t-test (GraphPad Prism 9

software; *, $p<0.05$; **, $p<0.01$). The PhenoGraph UMAP plots in (I) show the position (green) and frequency of B cells in Cluster 'a', which represents a population of ABCs expanded in Active cGVHD (**fig. S2**). In (J), histogram overlays for TACI surface protein expression on B cells in the six clusters from the PhenoGraph assessment described as being designated $TACI^{Br}$ (**fig. S2**), from the 4 allo-HCT patients in each group. Arrows for Clusters 'k', 'j' and 'n' highlight elevated TACI expression levels observed in some Active cGVHD patients. (**K**) B cells positive for *TNFRSF13B* (*TACI*) transcripts appear elevated in Active cGVHD patients. Normalized expression of *TNFRSF13B* in UMAP space are shown, separated by patient group. Boxed areas in representative regions (I, II) are enlarged to show detail.

The circulating 'memory' B cell compartment in allo-HCT patients is distinct from HDs and non-HCT patients

Since allo-HCT patients had reduced DP ($CD27^+CD11c^+$) B cells (**Fig. 3B,C**), we next assessed 'memory' B cell gene profiles in allo-HCT compared to HD or individuals with non-HCT chronic diseases. For this we leveraged a similar, publicly-available scRNA-Seq dataset generated from blood B cells of HDs (*n*=3) and non-HCT patients chronically exposed to HIV (*n*=3) or malaria (*n*=3), published by Holla et al. (*29*). We first identified total *CD27*$^+$*ITGAX*$^-$, *CD27*$^-$*ITGAX*$^+$, and *CD27*$^+$*ITGAX*$^+$ B cells from all patient and HD groups (described in the Methods section) to match the same subsets defined by flow cytometry (**Fig. 3B,C**). We then assessed the frequency of B cells within these Cluster 5 subsets that expressed other genes associated with the function or additional phenotype(s) of memory B cells (*51-54*). Displaying the frequency of positive B cells as a heat map (**fig. S4**), we found that most genes were similar between all 5 groups. However, certain genes were remarkably distinct in allo-HCT patients, irrespective of cGVHD status, when compared to either HDs, HIV patients or malaria patients (**Fig. 4**). B cells expressing *ADA* [associated with a form of SCID with disrupted B cell tolerance (*55*)], the T cell-attracting chemokine *CCL22* (*56*), and 3 G-protein coupled receptors (GPCRs) important for B cell exit from the BM and/or homing to SLO niches, *CCR7*, *S1PR1*, and *S1PR2* (*57-61*), were increased in frequency across *CD27*/*ITGAX* subsets in allo-HCT patients. B cells expressing *ITGB2*, which pairs with various integrin alpha chains to mediate migration, and is a potential marker of ABCs (*29*), were proportionally decreased in allo-HCT patients. *CD27*/*ITGAX* subsets in allo-HCT patients also had broadly increased proportions of B cells expressing survival regulators with known roles in memory B cell maintenance including *BCL2* (*62*) and *TRADD* (*63*). By contrast, allo-HCT patients had a paucity in B cells expressing *FOS*, important during the GC response and

terminal differentiation to plasma cells (*64*). Together these data reveal that the memory B cell pool in allo-HCT possesses intrinsic molecular hallmarks of altered tolerance, migration, SLO homing, and survival.

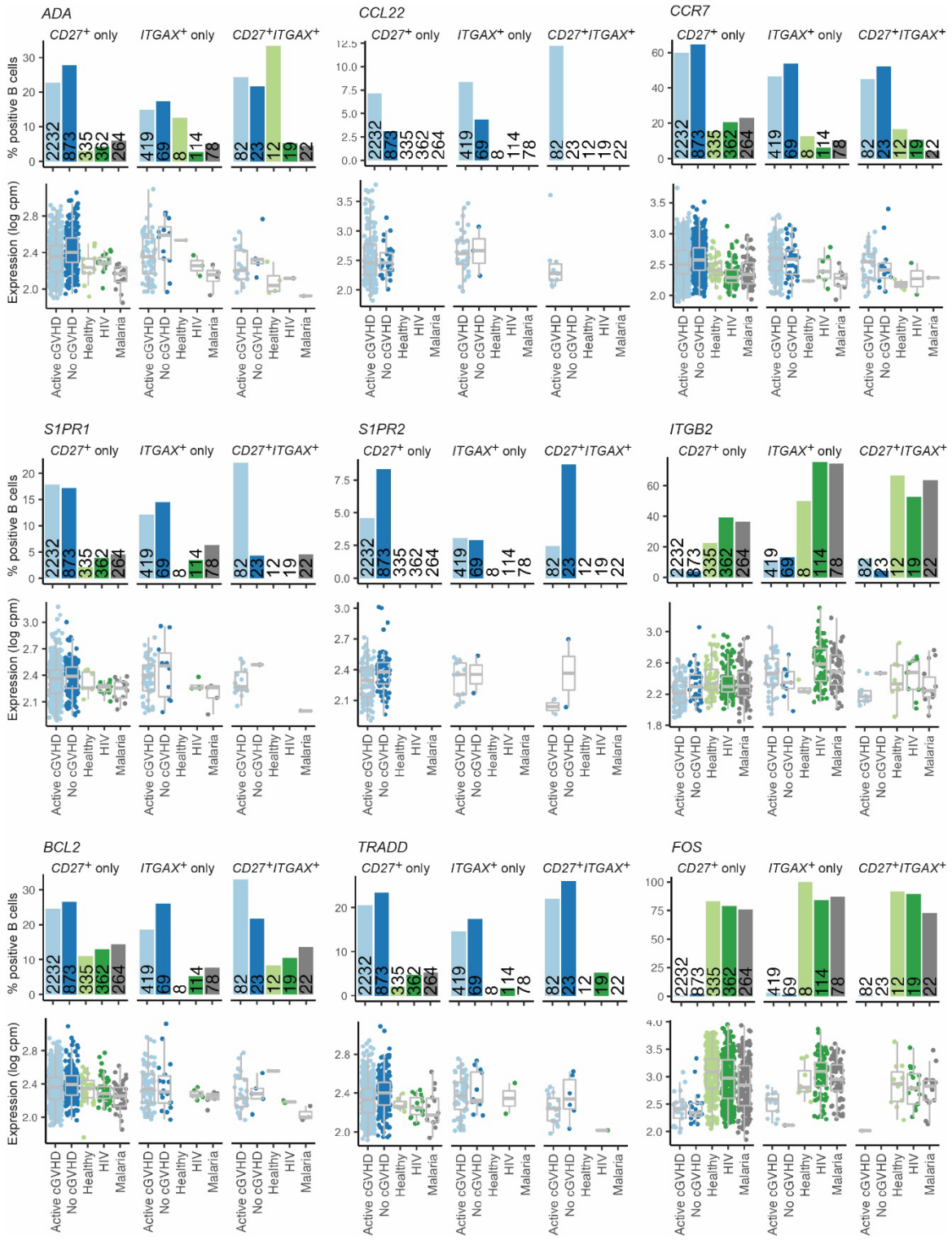

Fig. 4. 'Memory' *CD27* and *ITGAX* B cell subsets are transcriptionally unique in allo-HCT patients compared to HDs and non-HCT patients. Shown are results for 9 'memory' B cell

genes of interest displaying differences in the frequency of positive B cells between allo-HCT patients compared to HD (Healthy) and non-HCT patient groups (HIV, Malaria). Bar graphs represent the % positive B cells for the population indicated. Numbers embedded within the bars indicate the total number of B cells identified within the subset indicated, for the patient or HD group. In the gene expression graphs below each bar graph, each point represents an individual B cell, with the data normalized to show expression values for the gene of interest per million total mapped reads in the same B cell, expressed on a log scale (log CPM).

Genes critical for B cell fate and function are differentially expressed in Active cGVHD

Having determined signature gene features of the allo-HCT B cell compartment, we next focused on differentially expressed genes (DEGs) between allo-HCT patient groups (Active cGVHD vs. No cGVHD). In **Fig. 5**, bar graphs represent total DEGs by cluster, either increased (Up, **Fig. 5A**) or decreased (Down, **Fig. 5B**) in Active cGVHD. Cluster 9, previously inferred to be the metabolically activated (**Fig. 2**) had the greatest number of Up DEGs in Active cGVHD (193). Cluster 5, inferred to be the memory/ABC subset (**Fig. 1H**, **Fig. 2A**), had the greatest number of Down DEGs (335). From the total list of DEGs (**table S3**), we first focused on genes with known functional roles in B cells ('Select' DEGs). As shown in the heatmaps in **Fig. 5C,D**, a relatively large number of select DEGs occurred in at least one B cell cluster. We further categorized these DEGs according to their known roles in B cell function (**Fig. 5E**). Some DEGs in Active cGVHD patient B cells suggested aberrant migration and homing. For example *CXCR4*, a regulator of B cell migration from the BM to the periphery (*65*), was increased in transitional B cell Clusters 1, 2 and 4 (**Fig. 5C,E**). Active cGVHD B cells also had Up DEGs for other GPCRs known to regulate B cell homing and retention within essential SLO niches, including *GPR183* (i.e., *EBI2*), *P2RY8*, *S1PR2*, and *CXCR3* (*59, 66-69*). *GPR183/EBI2* was notably increased across five B cell clusters (**Fig. 5C,E**), including the transitional-like subsets (Clusters 1 and 2) and the memory/ABC subset (Cluster 5). This was a potentially important finding because EBI2 has an intricate role in regulating B cell movement within the follicle before and following the GC reaction (*66, 69*). *P2RY8* and *S1PR2* were both Down DEGs in activated Cluster 9 and/or 'memory' Cluster 5 (**Fig. 5D,E**), intriguing since these molecules are also pivotal in B cell homing and confinement to follicular niches or the GC reaction (*59, 68, 70*), and decreased *P2RY8* expression is linked to pathogenic antibody production and expansion of plasma cells and ABCs

in humans and mice (*71*). Our DEG data thus suggest altered follicle and GC movement of B cells in human cGVHD, consistent with findings in cGVHD mouse studies (*3, 17, 72*).

Other notable Down DEGs in Active cGVHD B cells (**Fig. 5D,E**) included (in 5 clusters) *CD83*, known for discriminating light and dark zone B cells within GCs (*73*). *IL21R* was decreased in Clusters 3 and 10, potentially important since interleukin (IL)-21 is critical to the humoral immune response and the development of regulatory B cells (Bregs), and Bregs are reduced in Active cGVHD patients (*5*). *FAS* was decreased in Cluster 5, along with decreased *TRADD* in both Cluster 5 and metabolically active Cluster 9, suggesting disruption of important mediators of apoptosis and potentially impaired elimination of autoreactive B cells (*74*). *SLAMF7* (*CRACC*, *CD319*) was also notable since it can positively regulate B cell proliferation and cytokine production (*75*), being an Up DEG in Cluster 9 (**Fig. 5C,E**).

Given a potentially prominent role for BAFF in the genesis and progression of cGVHD (*7, 8, 10, 11, 76*), it was notable that the BAFF receptor *TNFRSF13B* (*TACI*) was increased in Clusters 8 and 10 (**Fig. 5C,E**). Other members of the TNF superfamily (TNFSF) or TNF-receptor superfamily (TNFRSF) involved in key B cell pathways were likewise Up DEGs in Active cGVHD B cells, including *TNFRSF14* (*LIGHTR*, *CD270*), *TNFSF10* (*TRAIL*, *CD253*), *TNFRSF12A* (*FN14*, *TWEAKR*, *CD266*), *TNFRSF1B* (*TNFR2*, *CD120b*), and *TNFRSF10B* (*TRAILR2*, *CD262*), **Fig. 5C,E**. Interestingly, *GPR183* (*EBI2*) was overexpressed in Cluster 8 along with *TNFRSF13B* (**Fig. 5C,E**; **fig. S5A**), possibly reflecting a positive influence by BAFF on EBI2 expression, as reported (*77*). Co-expression of *GPR183* and *TNFRSF13B* indeed occurred in some B cells, which were expanded 4-fold in Active cGVHD patients (**fig. S5B,C**). Indeed EBI2, like TACI, was expressed at a high level on the surface of CD11c$^+$ ABCs by flow cytometry (**fig. S5D**), while follicular-like naïve B cell subsets were generally low/negative for EBI2 and

TACI expression (**fig. S5E**). Thus our data add new insight to the recent finding that *TNFRSF13B* and *GPR183* are major DEGs defining a B cell branch point that immediately precedes ABC expansion in adults chronically exposed to malaria antigens (*29*).

Regulators of upstream BCR signaling, *BTK* and *BLNK*, were Up DEGs in Active cGVHD, including 'memory' Cluster 5 (**Fig. 5C,E**). This is consistent with work showing BAFF-dependent increases in BLNK protein in B cells from Active cGVHD patients and mice (*8, 16*). The transcription factor *ZBTB20* was increased in pre-GC-like Cluster 10, and this zinc finger protein is essential for the conversion of BCR-activated B cells to antibody-secreting cells (ASCs) and maintenance of long-lived ASCs (*78*). *CAV1* (*CAVEOLIN-1*), a molecule that controls BCR compartmentalization on the plasma membrane (*79*), was decreased in Clusters 1 and 10 (**Fig. 5D,E**). Accordingly, *Cav1* deficiency in mice leads to altered nanoscale organization of IgM-BCRs and a skewed Ig repertoire with features of poly-reactivity and auto-reactivity (*79*). Molecules shown to be functionally important in ABC expansion or function were also significantly affected. *ZC3H12A*, which encodes the RNA-binding protein REGNASE-1, was decreased in Cluster 1 (**Fig. 5D,E**), and Regnase-1 deficiency at earlier stages of B cell development in mice produces severe autoimmune immunopathology and early mortality, accompanied by ABC expansion (*80*). *TBX21* (encoding *TBET*), *ZEB2* and *EGR3* are important and potential master regulators of ABC development and/or function in mice and humans (*22, 24, 25, 47*), and each were Up DEGs in either 'memory' Cluster 5 (*TBX21*, *ZEB2*) or activated Cluster 9 (*EGR3*), **Fig. 5C,E**. Cluster 5 was enriched for ABCs (**Fig. 3A**), suggesting that dysregulated *TBET*, *ZEB2* and *EGR3* are potential drivers of the observed ABC expansion in Active cGVHD patients (**Fig. 3B-I**). Finally, a set of genes associated with cell cycle were among the observed DEGs in Active cGVHD. These included *CDKN1B* and *CCND3* (Up, **Fig. 5C,E**), and *CDKN1A* (Down, **Fig. 5D,E**). This was

consistent with our previous observations that Active cGVHD B cells demonstrate enhanced proliferation to some important stimuli, including low-dose surrogate antigen and NOTCH ligand (*8, 9*). Together these data define new aspects of B cell subsets following allo-HCT, whereby distinct maturation, activation, survival and homing pathway alterations occur when B cell tolerance is not achieved in the form of cGVHD.

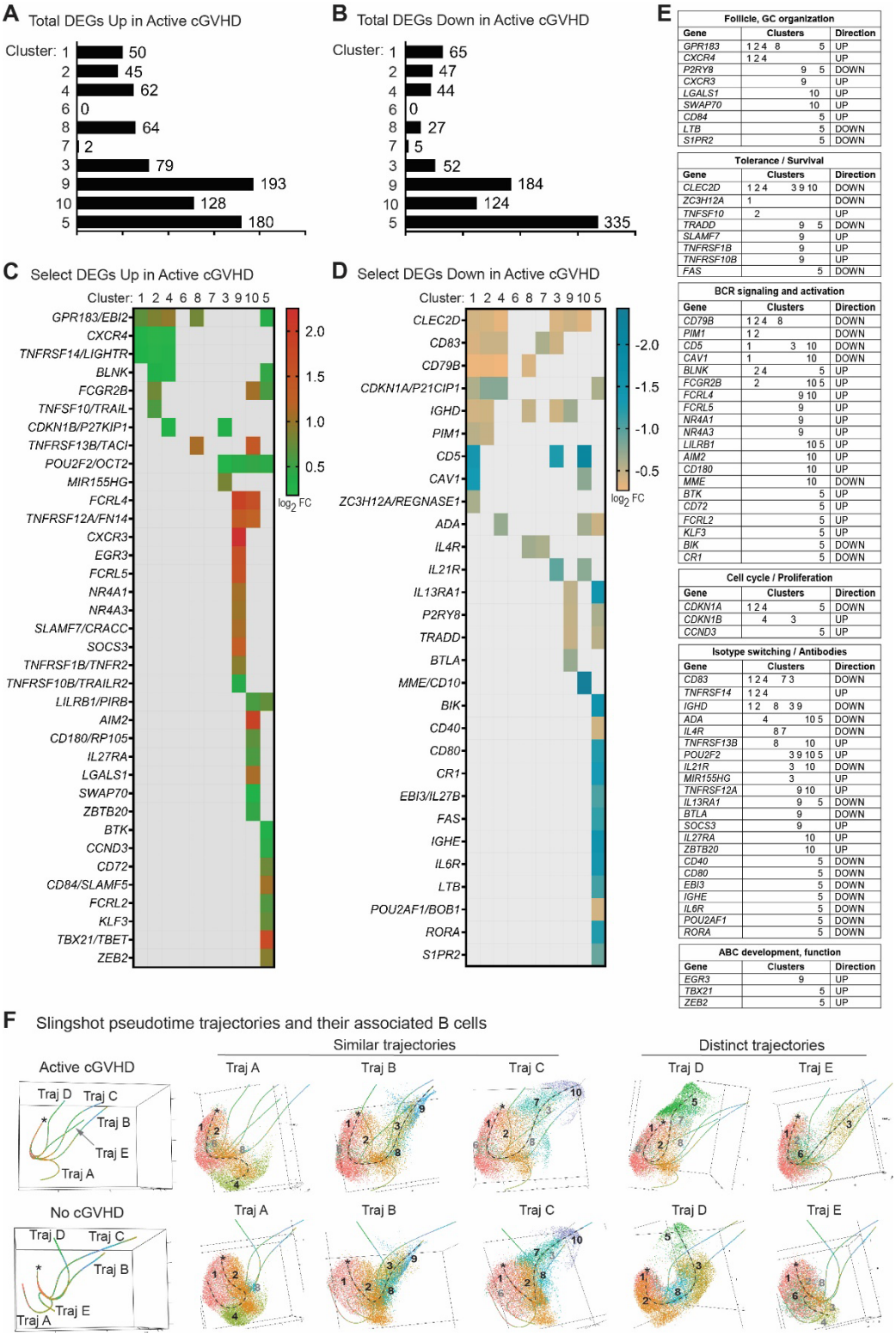

E

Follicle, GC organization		
Gene	Clusters	Direction
GPR183	1 2 4 8 5	UP
CXCR4	1 2 4	UP
P2RY8	9 5	DOWN
CXCR3	9	UP
LGALS1	10	UP
SWAP70	10	UP
CD84	5	UP
LTB	5	DOWN
S1PR2	5	DOWN

Tolerance / Survival		
Gene	Clusters	Direction
CLEC2D	1 2 4 3 9 10	DOWN
ZC3H12A	1	DOWN
TNFSF10	2	UP
TRADD	9 5	DOWN
SLAMF7	9	UP
TNFRSF1B	9	UP
TNFRSF10B	9	UP
FAS	5	DOWN

BCR signaling and activation		
Gene	Clusters	Direction
CD79B	1 2 4 8	DOWN
PIM1	1 2	DOWN
CD5	1 3 10	DOWN
CAV1	1 10	DOWN
BLNK	2 4 5	UP
FCGR2B	2 10 5	UP
FCRL4	9 10	UP
FCRL5	9	UP
NR4A1	9	UP
NR4A3	9	UP
LILRB1	10 5	UP
AIM2	10	UP
CD180	10	UP
MME	10	DOWN
BTK	5	UP
CD72	5	UP
FCRL2	5	UP
KLF3	5	UP
BIK	5	DOWN
CR1	5	DOWN

Cell cycle / Proliferation		
Gene	Clusters	Direction
CDKN1A	1 2 4 5	DOWN
CDKN1B	4 3	UP
CCND3	5	UP

Isotype switching / Antibodies		
Gene	Clusters	Direction
CD83	1 2 4 7 3	DOWN
TNFRSF14	1 2 4	UP
IGHD	1 2 8 3 9	DOWN
ADA	4 10 5	DOWN
IL4R	8 7	DOWN
TNFRSF13B	8 10	UP
POU2F2	3 9 10 5	UP
IL21R	3 10	DOWN
MIR155HG	3	UP
TNFRSF12A	9 10	UP
IL13RA1	9 5	DOWN
BTLA	9	DOWN
SOCS3	9	UP
IL27RA	10	UP
ZBTB20	10	UP
CD40	5	DOWN
CD80	5	DOWN
EBI3	5	DOWN
IGHE	5	DOWN
IL6R	5	DOWN
POU2AF1	5	DOWN
RORA	5	DOWN

ABC development, function		
Gene	Clusters	Direction
EGR3	9	UP
TBX21	5	UP
ZEB2	5	UP

Fig. 5. Molecules critical to B cell function are altered within clusters in Active cGVHD. (**A-D**) DEG analysis within the 10 B cell clusters in the scRNA-Seq dataset based on disease status

(as described in **Fig. 1**: Active cGVHD, *n*=4; No cGVHD, *n*=4). Bar graphs indicate the total number of DEGs by cluster Up (A) or Down (B) in Active cGVHD. The heat maps in (C) and (D) depict DEGs selected from the entire dataset (**table S3**), critical for various aspects of B cell function ('Select' DEGs). Colored squares represent significant (P_{adj} <0.05) log2 fold change (log2 FC) values for DEGs shown (rows) within the cluster(s) indicated (columns), either Up (C) or Down (D) in Active cGVHD B cells. (**E**) All genes from (C) and (D) were grouped into the major categories shown based on their known roles in B cell function. The clusters in which each gene was significantly altered are summarized in the middle column, with the direction of change in Active cGVHD B cells relative to No cGVHD B cells indicated in the right column. (**F**) The panels at left show Slingshot pseudotime trajectory predictions (Traj A-E) for untreated B cells from Active cGVHD patients (top) and No cGVHD patients (bottom). The origin of the pseudotime analysis (asterisks) was set as Cluster 1 based on our knowledge of its transitional, Igκ signature gene profile (**Figs. 1E,F** and **2A,B**), suggesting it is the earliest peripheral B cell population emerging from the bone marrow. Panels at right for each patient group represent each trajectory in isolation (dashed line for reference), along with all of its associated B cells. B cells clusters are colored and numbered per original unbiased clustering (**Fig 1B,C,I**). Black numbers indicate major clusters that lie along each trajectory, while clusters present but having only a small number of B cells represented are indicated in gray.

Lesional skin B cells in Active cGVHD share characteristics of hyper-activity with circulating B cell subsets

Certain DEGs in B cells that circulate in Active cGVHD patients suggest that these cells may home to sites of disease involvement. Thus, we performed scRNA-Seq on a punch biopsy of lesional skin (dermis) from a patient with sclerodermatous cGVHD and compared it with a biopsy of normal dermal skin from a HD undergoing abdominoplasty. Dermal B cells were detected in both samples, and were distinguishable by a single UMAP cell cluster plus signature gene profile (**table S4**), which indicated the presence of Igκ (*IGKC*), mostly isotype-switched (*IGHG1*, *IGHG3*, *IGHG4*, *IGHA1*) B cells. Other notable signature genes included *GPR183* (*EBI2*) and receptors for BAFF (*TNFRSF13B* [*TACI*] and *TNFRSF13C* [*BAFFR*]). Remarkably, multiple Up DEGs in blood B cell clusters in Active cGVHD patients (**Fig. 5C,E**) were also Up DEGs in Active cGVHD sclerodermatous skin B cells (**table S5**). *POU2F2* (*OCT2*), important for generation of ASCs (*81*), *SWAP70*, a molecule phosphorylated by SYK that influences B cell migration and ABC expansion (*82, 83*), and *AIM2*, which has a positive role in the expansion of autoreactive B cells in a mouse lupus model (*84*), were increased in both blood and skin B cells in Active cGVHD. Not surprisingly, most DEGs observed in sclerodermatous skin that were also DEGs in blood B cells of Active cGVHD patients occurred in the most activated and differentiated blood B cell clusters, primarily Clusters 3, 9, 10 and 5 (**Fig. 5C,E**, **table S3**, **table S5**).

Trajectories for B cell subset diversification in Active cGVHD patients reflect maturation defects that can potentially be corrected

Our past findings (*9*) suggest that altered maturation is linked to aberrant activation of circulating Active cGVHD B cells. Thus, we performed pseudotime trajectory analysis of our scRNA-Seq

dataset using Slingshot (*85*), which may provide insight into the diversification of B cell subsets as they diversify or reach various states of activation. As shown in **Fig. 5F** (far left panels), our analysis predicted 5 pseudotime trajectories (designated Traj A-E) for each allo-HCT patient group. Asterisks indicate the origin (starting point) for the trajectories based on 'biological knowledge', assigned to Cluster 1 because of its transitional-like, *IGKC* (Igκ^{+}) phenotype. Traj A, B and C were remarkably similar between allo-HCT patient groups (**Fig. 5F**, 'Similar trajectories'). Traj A consisted primarily of B cell Clusters 1, 2, and 4 only, possibly indicating termination at Cluster 4 that had generally low transcripts, consistent with a state of B cell anergy, (**Fig. 1E**). Traj B proceeded through Clusters 1, 2, 8, 3, and 9. Traj C proceeded through Clusters 1, 2, 8, 7, and 10, although in Active cGVHD there were notably fewer B cells in Cluster 8 (apparent minor contribution indicated by gray font). Traj D and E were markedly different between patient groups (**Fig. 5F**, 'Distinct trajectories'). In No cGVHD, Traj D had clear progression through Clusters 1, 2, 8, 3 and 5. By contrast in Active cGVHD, Traj D completely lacked Cluster 3 and had minimal Cluster 8 B cells, proceeding primarily through Clusters 1 and 2, then directly to Cluster 5. Traj E had major contributions from Clusters 1 and 6 in both groups, while Cluster 3 was uniquely prominent in Active cGVHD. These observations suggest that the generation of Cluster 5 'memory' B cells in Active cGVHD patients can potentially occur along a diversification pathway that bypasses tolerance checkpoints, represented by Cluster 8 and Cluster 3 in No cGVHD where tolerance is achieved.

The DEGs and altered trajectories described above expand on our previous study demonstrating a maturation block in circulating B cells in Active cGVHD patients (*9*). Previously, we utilized all-*trans* retinoic acid (ATRA) as a tool *in vitro* to 'mature' Active cGVHD B cells by restoring a normal IRF4/IRF8 ratio, attenuating hyper-responsiveness to BCR and NOTCH co-

stimulation (*9*). Thus, we assessed the effects of ATRA on B cell clustering, DEGs, and trajectory inferences. A total of 10,000 ATRA-treated B cells per sample were targeted for scRNA-Seq analysis, from the same 8 allo-HCT donor patients described in **Fig. 1** and **table S1**. ATRA treatment efficacy was validated by the robust upregulation of known ATRA-responsive genes across multiple B cell clusters including *PLAAT4* (i.e., *RIG1*, *Retinoid-Inducible Gene 1*) and *ASB2* (*86*) [**table S6**]. ATRA treatment resulted in four predicted pseudotime trajectories (designated A-D) in both allo-HCT patient groups (**Fig. 6A,B**), compared to the five trajectories for untreated B cells (**Fig. 5F**), suggesting a potential narrowing of transcriptional diversity. Supporting this, Cluster 8 was notably absent from the post-ATRA UMAP clusters, while the nine remaining clusters were present (**Fig. 6C,D**). Remarkably, the trajectory leading to Cluster 5 in ATRA-treated Active cGVHD B cells (Traj D, **Fig. 6A**) included Clusters 1, 2, 7, 3, 10 and 5, which was a markedly different profile from the trajectory leading to Cluster 5 in untreated Active cGVHD B cells (Traj D, **Fig. 5F** top panel). This suggests that ATRA, to some extent, normalized the trajectory leading to ABCs and memory B cells when cGVHD was clinically apparent. In all scenarios with ATRA treatment, Cluster 3 preceded Clusters 9, 10 and 5, implicating this subset as a pivotal precursor memory checkpoint population.

ATRA affected the distribution of some B cell populations differently between patient groups. The ratio of B cells mapping to Clusters 1 and 2 was much lower for No cGVHD B cells (0.38 and 0.43, respectively) compared to Active cGVHD B cells (0.84 and 0.79, respectively) following ATRA treatment (**Fig. 6C,D**). The ratios of B cells mapping to Clusters 7 and 3 were reciprocally changed between groups by ATRA, decreasing in No cGVHD (0.76 and 0.93, respectively) and increasing in Active cGVHD (1.23 and 1.51, respectively). These differences may be explained, at least in part, by reduced viable B cells with ATRA treatment in No cGVHD

compared to Active cGVHD (ATRA/Untr total B cell ratio of 0.70 for No cGVHD vs. ATRA/Untr total B cell ratio of 0.93 for Active cGVHD, **Fig. 6C,D**).

Finally, assessment of DEGs following ATRA treatment revealed altered expression of a multitude of genes compared to untreated B cells from all 8 allo-HCT patients (**table S6**), although these DEG changes were statistically indistinguishable between groups based on cGVHD disease status. Total DEGs decreased or increased by ATRA are represented numerically in **Fig. 6E** and **6G**, respectively. Cluster 7 was most affected by ATRA, with 1,673 Down DEGs compared to untreated B cells (**Fig. 6E, table S6**). Interestingly, some DEGs in untreated B cells from Active cGVHD patients (Up or Down compared to No cGVHD, **Fig. 5C-E**) were significantly changed in the opposite direction by ATRA (**Fig. 6F,H**), hinting at potential corrective effects by agents that promote B cell maturation. Both *GPR183* (*EBI2*) and *TNFRSF13B* (*TACI*) were decreased upon ATRA treatment across multiple clusters, representing both 'transitional' Clusters 1 and 2, and 'memory' Cluster 5 (**Fig. 6F**). Thus, ATRA both reshaped the distribution of B cells among clusters and impacted the transcription of some DEGs observed in Active cGVHD.

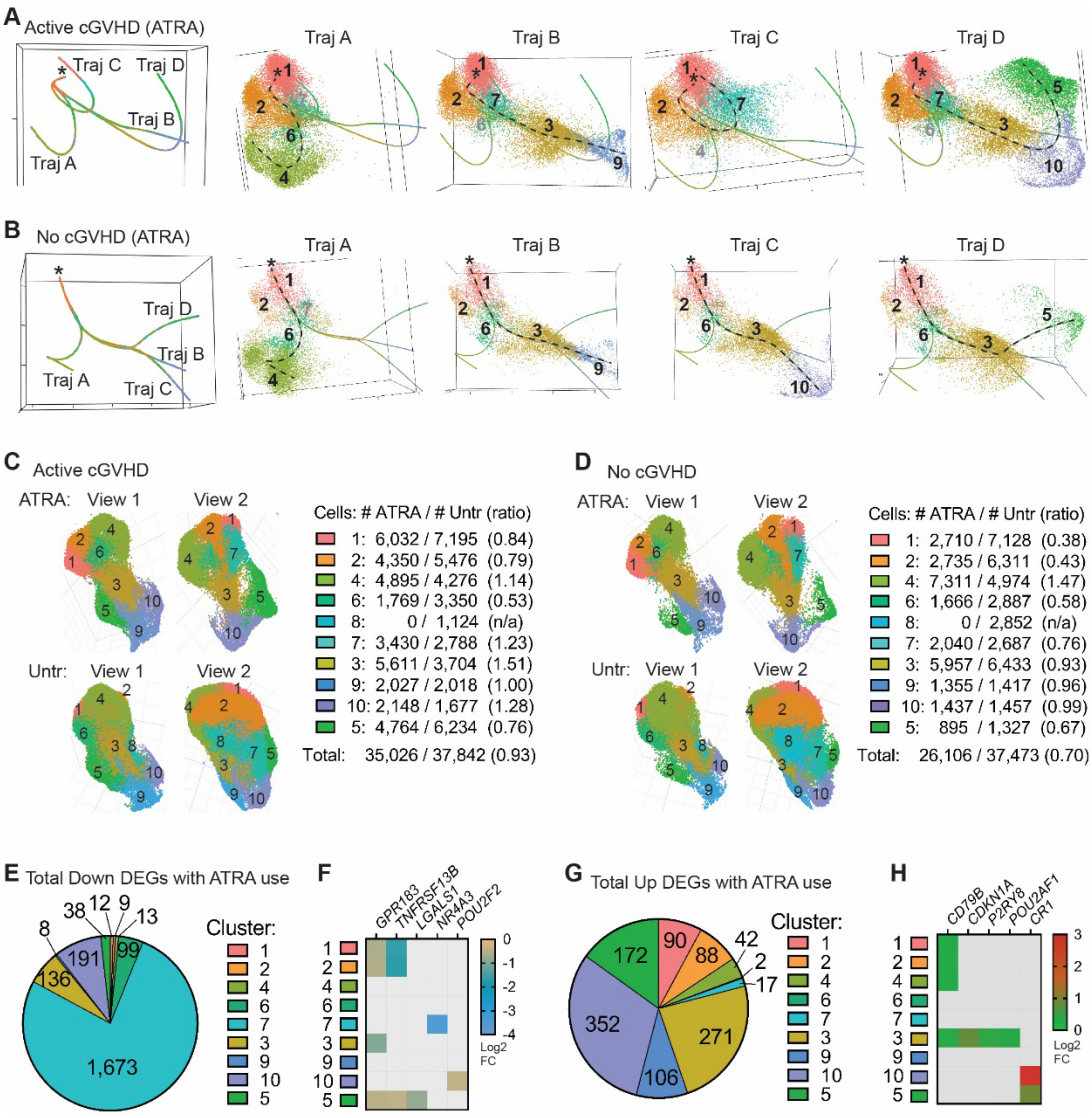

Fig. 6. An inducer of cell differentiation, all-*trans* retinoic acid (ATRA), differentially influences B cell pseudotime trajectories and cluster distribution in Active cGVHD. (**A,B**) Panels at left show trajectory estimates (Traj A-D) for B cells from Active cGVHD patients (A) and No cGVHD patients (B) after treatment with ATRA for 18 h. The origin (asterisks) was set as Cluster 1, as in **Fig. 5F**. Panels at right for each patient group represent each trajectory in isolation (dashed line for reference), along with all of its associated B cells. B cells are colored and numbered by the cluster to which they belong. Black numbers indicate major clusters that lie along each trajectory, while clusters present but having only a small number of B cells represented are

indicated in gray. (**C,D**) ATRA effects on B cell distribution among clusters relative to untreated B cells. UMAP cluster projection and B cell distribution per cluster among ATRA-treated and untreated (Untr) Active cGVHD samples (C), and among ATRA-treated and untreated (Untr) No cGVHD samples (D). Total B cell numbers within each cluster for each treatment group and patient group are indicated. For ATRA-treated B cells, the 9 clusters shown were identified as corresponding to the same 9 clusters in the untreated groups based on signature gene profiles. Ratios represent the number of B cells with ATRA treatment divided by the numbers of B cells for untreated cells (#ATRA / #Untr). (**E-H**) DEGs induced by ATRA in B cells from all 8 allo-HCT patients in the single-cell RNA-Seq dataset, compared to untreated B cells from all 8 patients. Pie charts indicate the total number of DEGs significantly decreased (E) or increased (G) after ATRA treatment in the cluster indicated. Heat maps (F and H) represent DEGs from **Fig. 5** that were significantly altered in the opposite direction following ATRA treatment. Colored squares represent significant (P_{adj} <0.05) log2 FC value for the gene and cluster indicated, for ATRA-treated B cells (all 8 samples) compared to untreated B cells (all 8 samples).

Some genes are broadly dysregulated across B cell populations in Active cGVHD patients

B cells from Active cGVHD patients are generally hyper-responsive to surrogate antigen (*9, 16*). We thus hypothesized that some DEGs occur broadly in this disease, which might affect B cells at multiple stages of peripheral diversification. In **Fig. 7A** we show Up DEGs (left) and Down DEGs (right) in the scRNA-Seq dataset that occurred in at least 4 B cell clusters in untreated Active cGVHD B cells. DEGs were ranked based on occurrence in the most clusters, and then by their first occurrence in the least mature/activated clusters. Twenty-nine DEGs were increased and 34 DEGs were decreased in 4 or more clusters in Active cGVHD. Several of these DEGs were already depicted in **Fig. 5C-E** because of their known role in B cell function (bold font in **Fig. 7A**). To corroborate broad dysregulation we also subjected the scRNA-Seq dataset to a 'bulk-like' DEG analysis (all B cells, **Fig. 7B**). Indeed, numerous DEGs from **Fig. 7A** were also significant the bulk-like analysis (**Fig. 7B**, asterisks). We grouped the DEGs from **Fig. 7B** empirically into GO-annotated cellular pathways to further highlight potential function (**table S7**). *ARRDC3* was among the most broadly decreased DEGs in Active cGVHD B cells (**Fig 7A,B**). Although the function of this α-arrestin in B cells is unknown, this finding further highlights the potential for dysregulation of GPCRs in Active cGVHD. Also notable, *NFKBIA* (encoding IκBα, the inhibitor of NFκB signaling), was decreased in eight clusters. By contrast, *CKS2* stood out among the most broadly increased DEGs in Active cGVHD B cells, reaching significance in eight clusters (**Fig. 7A**) and in the bulk-like analysis (**Fig. 7B**).

CKS2 is important for cell cycle, serving as a co-activator of cyclin-dependent kinases (CDKs) (*87*). Alternatively, CKS2 can prevent or delay cell cycle progression by protecting the CDK inhibitor $P27^{KIP1}$ (CDKN1B) from proteasomal degradation by competing with proteins that recruit ubiquitin ligases (*88*). This protection of $P27^{KIP1}$ from degradation by CKS2 averts

premature cell cycle entry, preventing apoptosis (*89*). UMAP plot comparisons clearly depict the widespread increase in *CKS2*-positive B cells in Active cGVHD (**Fig. 7C**). Displayed as normalized expression values (**Fig. 7D**), *CKS2* was uniformly increased in Active cGVHD samples in the eight clusters reaching significance (Clusters 1,2,4,8,3,9,10&5). We further validated this *CKS2* finding by qPCR analysis on purified B cells from an independent cohort of allo-HCT patients (**Fig. 7E**, **table S2**).

Given that Active cGVHD B cells have enhanced survival in culture (*7*), *CKS2* being broadly increased hinted that $P27^{KIP1}$ may be more protected from degradation. If so, $P27^{KIP1}$ may exhibit elevated phosphorylation at T198, a site where CKS2 competes for binding with ubiquitin ligase complexes (*88*). Employing unbiased protein phosphoarrays and whole cell lysates from purified B cells of an independent cohort of allo-HCT patients, phospho-T198 was detected at a 6- to 10-fold greater level in Active cGVHD B cells compared to No cGVHD B cells (**Fig. 7F,G** and **fig. S6**). Active-site phosphorylation on the kinases AMPK and RSK, known to phosphorylate $P27^{KIP1}$ T198 (*90, 91*), were similar between allo-HCT patient B cells, suggesting that increased kinase activity was not responsible for enhanced phospho-T198 in Active cGVHD. Analysis of total protein supported the concept of $P27^{KIP1}$ being protected in Active cGVHD B cells, with levels remaining higher compared to No cGVHD B cells (**Fig. 7H**). A model for potential $P27^{KIP1}$ regulation in Active cGVHD B cells is shown in **Fig. 7I**, whereby broadly increased CKS2 expression, combined with increased *CDKN1B* (*P27KIP1*) transcription in some subsets (**Fig. 5C,E**), may lead to $P27^{KIP1}$ accumulation. Thus, our dataset allows us to begin to determine functional contributors of enhanced B cell survival in Active cGVHD, and supports prior work showing that cGVHD B cells are primed for proliferation and protected from apoptosis (*7, 9, 16*).

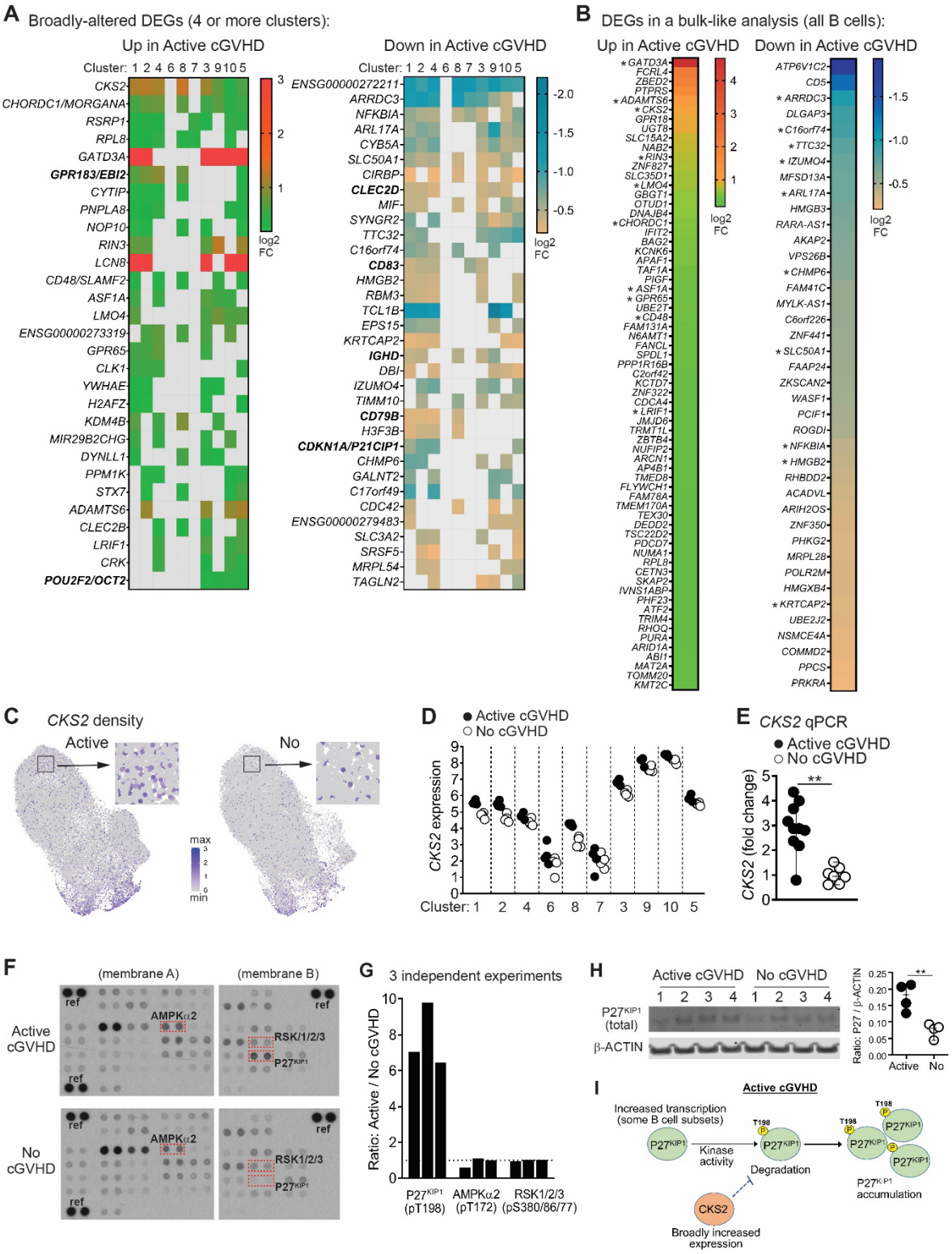

Fig. 7. Assessment of broadly-altered DEGs provides additional insight into altered B cell functions in Active cGVHD. A, DEGs in the scRNA-Seq dataset reaching significance (P_{adj}

<0.05) in four or more B cell clusters as described in **Fig. 5**, either Up (left heat map) or Down (right heat map) in Active cGVHD. Colored squares indicate significance, with log2 FC values as indicated. No DEGs mapped to Cluster 6. Genes also depicted in **Fig. 5C-E** are shown in bold font. **B,** DEG analysis performed on total untreated B cells. Heat maps show log2 FC values for genes with statistically different (P_{adj} <0.05) expression between allo-HCT patient groups (Up or Down in Active cGVHD, as indicated). **C-E,** Validation of *CKS2* transcript overexpression in Active cGVHD B cells. In (C), normalized expression density UMAP plots for *CKS2* between Active cGVHD (Active) and No cGVHD (No) are shown. Representative regions (boxes) were chosen randomly and enlarged (arrows) to visualize single B cells more easily. In (D), normalized *CKS2* expression values across all 10 B cell clusters for all 8 allo-HCT patients are shown, separated by disease group. In (E), qPCR analysis of *CKS2* was performed on untreated B cells from a different allo-HCT patient cohort having Active cGVHD (*n*=10) or No cGVHD (*n*=7). Results indicate the fold change in *CKS2* expression based on the mean value in the No cGVHD group normalized to 1. *ACTB* (β-ACTIN) was the housekeeping gene. Statistical comparison was performed using a two-tailed Mann-Whitney test (GraphPad Prism 9 software; **, *p*<0.01). (**F**) Representative phosphoprotein capture arrays for detection of various intracellular signaling molecules phosphorylated on key sites, performed on whole cell lysates of purified, untreated B cells isolated from Active cGVHD (*n*=3) and No cGVHD (*n*=3) patient blood samples (see also **fig. S6**). Dashed boxes and protein IDs indicate the capture/detection location (duplicate spots) for $P27^{KIP1}$ (phospho-T198), AMPKα2 (phospho-T172), and RSK1/2/3 (phospho-S380/S386/S377, respectively). Reference control spots are indicated ('ref'). (**G**) Combined density results from the 3 independent phosphoprotein array assays shown in (F) and **fig. S6**. Each bar indicates the results from one experiment and represents the ratio of the average dual spot intensity for Active cGVHD

B cells over No cGVHD B cells (dashed line represents a ratio of 1 as a guide). (**H**) Western blot analysis of total $P27^{KIP1}$ protein levels relative to β-ACTIN in whole cell lysates of B cells isolated from Active cGVHD (*n*=4) and No cGVHD (*n*=4) patient blood samples. Statistical comparisons were performed using a two-tailed, unpaired t-test (GraphPad Prism 9 software; **, $p<0.01$). (**I**) Cartoon depiction of how CKS2 expression in Active cGVHD B cells may function via $P27^{KIP1}$ maintenance and accumulation.

The 'plastic' state of peripheral B cells following allo-HCT can be modeled based on our scRNA-seq data

Our previous work has suggested a non-static, 'plastic' molecular and functional state of peripheral B cells in allo-HCT, whereby maturation defects associate with cGVHD (*9*). Our scRNA-Seq dataset and supporting work provides new insight into these processes. Signature gene profiles defined 10 distinct B cell subsets (**Fig. 8, left**) that continually develop and circulate under constant exposure to alloantigens after allo-HCT. Allo-HCT patient 'memory' B cell subsets had some remarkably distinct gene features, regardless of cGVHD status, compared to the same subsets from healthy individuals or patients chronically exposed to microbial antigens ('non-HCT' setting). This suggests a unique "Allo-HCT Plasticity" involving altered migration and survival signals in the allo-HCT environment that may function to shuttle B cells more freely and aberrantly among the most diversified clusters, Clusters 5, 9 and 10 (**Fig. 8**, dashed 2-headed arrows). Thus, the peripheral B cell pool in allo-HCT patients is potentially 'malleable', and as such is possibly amenable to novel therapeutic strategies to prevent or treat cGVHD, while maintaining immunity against pathogens and malignant cells.

Our data also reveal gene alterations important for emergence and/or persistence of aberrantly activated B cells in allo-HCT, where cGVHD manifests. DEGs in Active cGVHD could be subdivided into two major categories (**Fig. 8**, right) that comprise intrinsic differences from a B-cell tolerant state (No cGVHD). The first category of DEGs emerge in B cells in early maturation states that are not constitutively activated ("Early Subsets", Clusters 1, 2, 4, 6, and 8). These genes are largely maintained as DEGs throughout B cell diversification ('Broadly-Altered'). The second category of DEGs seem to emerge only after some degree of BCR stimulation ("BCR-Activated", Clusters 3, 7, 9, 10 and 5). The observed expansion of potentially pathogenic ABCs in

Active cGVHD patients ("ABCs (including DN2) Expanded") is thus likely a consequence of gene alterations before and after BCR-engagement occurring in a cumulative way.

Altogether, new insight gained in our analyses herein enable new opportunities for exploitation of the identified molecular pathways to further understand tolerance loss in B cells, in allo-HCT and beyond. These molecular programs are possibly driven by extrinsic factors that alter trajectories for B cell diversification, impairing tolerance and expanding ABCs. The identification of these highly novel DEG profiles in cGVHD provides context for new avenues of exploration into mechanisms of B cell tolerance loss.

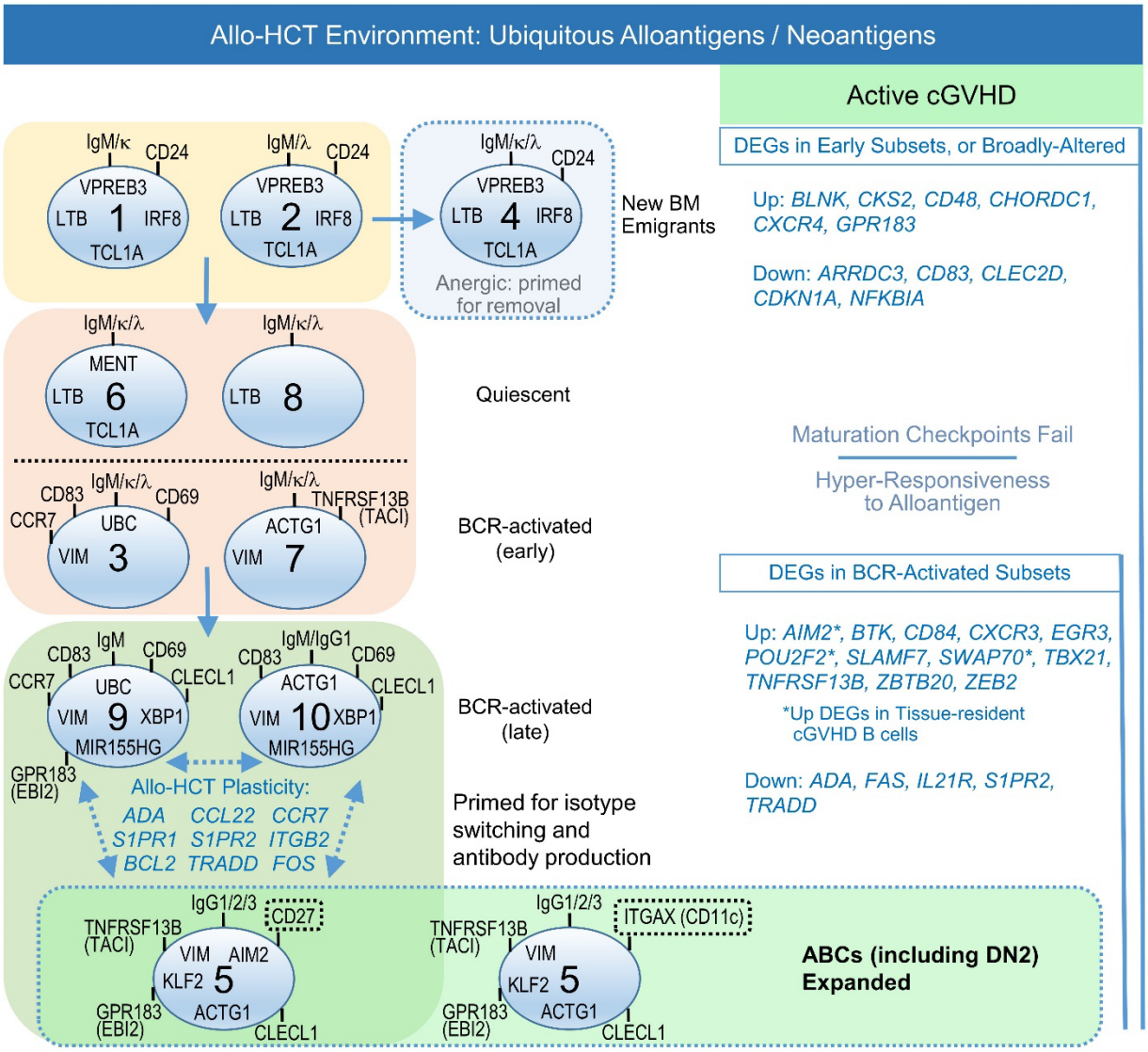

Fig. 8. Working model for extrinsic activation signals and intrinsic gene changes influencing B cell maturation, survival, and proliferative capacity that lead to the expansion of pathologic 'memory' B cells in Active cGVHD, including ABCs. Cluster-defining 'signature' genes (left side) and trajectory analyses (**Fig. 5F**) enabled the assignment of the 10 clusters along a logical pathway of B cell diversification in the periphery of allo-HCT patients, from newly-emigrated populations, through proposed checkpoint steps where survival decisions occur, and finally to BCR-activated and 'memory' states. As a culmination of extrinsic activation signals (ubiquitous alloantigens and soluble factors including BAFF), the allo-HCT environment becomes

amenable to gene changes generally, relative to non-HCT individuals (‘Allo-HCT Plasticity’). DEGs contributing to eventual pathogenesis occur early, broadly or exclusively after BCR stimulation, to promote Active cGVHD (right side).

DISCUSSION

Our scRNA-seq analysis reveals and details the breadth of B cell subset and gene expression abnormalities in human cGVHD. While immediate BCR hyper-responsiveness and aberrant upstream signaling in B cells from patients who manifest cGVHD has been shown (*7, 9, 16*), comprehensive analyses of the peripheral B cell compartment has been lacking. The clarity provided herein identifying signature genes that define individual B cell subpopulations, and DEGs associated with Active cGVHD, may support the development of improved targeted therapies for patients. Together these data demonstrate that early defects in the expression of some key genes will almost certainly alter the normal trajectory of B cells as they diversify, and be reflected in additional DEGs that lead to tolerance loss and host reactivity. We elucidate transcriptional programs that manifest and may lead to pathological functional changes in peripheral 'memory' B cell populations including ABCs. ABCs have emerged as important in both normal immunity and autoimmunity (*24, 25, 29, 30*). Indeed, transcriptional changes present in the earliest B cell subsets to inhabit the periphery are likely to influence the diversity and functional capacity of more mature or activated subsets, especially ABCs (including DN2) and other memory B cells. These subsets likely directly contribute to pathogenesis by producing alloantibodies after migrating to tissue sites where cGVHD manifests (*11*). Examples of unique transcriptional changes observed in our scRNA-Seq data included *CKS2* and *GPR183* (*EBI2*), each overexpressed in Active cGVHD from the earliest transitional/naïve B cell subsets to the most differentiated subset, Cluster 5, enriched for ABCs and $CD27^+$ memory B cells. Such DEGs occurring from (at least) the time B cells first enter the circulation may cause early epigenetic changes that alter subsequent tolerance checkpoints and potentially affect clonal diversity.

The expansion of ABCs (including DN2) with pathogenic roles in some disease settings, as we observed in Active cGVHD patients herein, is driven by one or more costimulatory signals that cooperate with BCR stimulation, including TLR7, IL-21 and IFNγ (*92-95*). Indeed, B cells isolated from Active cGVHD patients are hyper-responsive to minimal BCR ligation in synergy with co-stimulatory molecules including NOTCH2 and BAFF (*9*). These processes are likely driven in part by the increased BAFF-to-B cell ratio that occurs in cGVHD patients (*10, 11, 76, 96*), and by niche production of BAFF in the SLO, confirmed recently in a mouse cGVHD model (*8*). BAFF influence may additionally propagate by increases in BAFF receptors such as TACI (encoded by the *TNFRSF13B* gene), as published (*11*) and herein described for specific B cell subsets. It is also noteworthy that multiple other TNF superfamily and TNF-receptor superfamily members were increased DEGs in cGVHD B cell clusters, including the metabolically active Clusters 9 and 10. Some of these molecules (or their cognate receptors/ligands) are being evaluated as targets in clinical trials for autoimmune and inflammatory diseases, supporting the potential assessment in clinical trials for cGVHD as well. Thus, extrinsic factors in microenvironmental niches may be the initial drivers of DEGs that lead to early mechanisms of loss in peripheral B cell tolerance that can be elucidated through studies of circulating B cells.

Direct comparison of our allo-HCT patient scRNA-Seq dataset with a publicly-available dataset on blood B cells isolated from HDs and individuals with chronic infections (HIV, malaria), provided new insight into the unique aspects of the B cell pool that persists following immune reconstitution with allo-HCT therapy, regardless of cGVHD status. Some of these striking differences in the frequencies of B cells expressing molecules that orchestrate exit from the BM and homing to/establishment in SLO niches, along with molecules affecting survival, may impact the unique clinical manifestations of cGVHD once it occurs. These observations may additionally

reflect the apparent maturation block leading to B cell hyper-responsiveness in cGVHD patients (*9*), and may partially explain the paucity of $CD27^+$ follicular memory B cells in allo-HCT patients compared to HDs. Together these aspects of allo-HCT B cells hint at a unique opportunity for therapeutic targeting before cGVHD manifests.

Molecules identified in this study as dysregulated in subsets of Active cGVHD B cells are potentially novel, particularly molecules that regulate B cell movement and positioning within SLO. The identification of *GPR183* (*EBI2*), *P2RY8*, and *S1PR2* as each being dysregulated in one or more clusters of B cells is particularly remarkable, as each molecule is important for follicular movement and GC positioning of B cells (*59, 66-69*). The increase in *GPR183* across five B cell clusters, including transitional-like subsets, suggests that strictly regulated tolerance mechanisms that are initiated as B cells first recirculate and enter the SLO microenvironment may be disrupted in cGVHD patients. This is consistent with the notion that altered intrinsic functions of lymphocytes and stromal cells within SLOs disrupts normal architecture during follicle organization and GC development, potentially leading to premature displacement of B cells to extrafollicular spaces and altered tolerance (*72*). Remarkably, *GPR183*, *P2RY8*, and *S1PR2* were each DEGs in Cluster 5, which was enriched for ABCs and DN2. *P2RY8* expression was additionally decreased in metabolically active Cluster 9, intriguing given recent evidence that decreased B cell *P2RY8* propagates pathogenic antibody-producing plasma cells and ABCs in humans with lupus or antiphospholipid syndrome (*71*). The ligands for each of these molecules are known, and in some cases inhibitors and agonists have been described, permitting future studies in mouse models of cGVHD and eventually clinical trials. This concept is supported by an observation in a mouse lung transplant model of bronchiolitis obliterans (BO), a condition that frequently causes lung damage in cGVHD patients, where inhibition of GPR183 with a highly

selective inhibitor reduced pulmonary lymphoid lesions and lung damage (*97*). Elucidating B cell transcriptional changes that help incite cGVHD development, versus transcriptional changes that occur after cGVHD genesis and nevertheless contribute to ongoing pathogenesis in an unrelenting cycle, will remain an area of future investigation.

While the full implications of the findings herein are currently limited and remain to be realized in the clinical setting, our data provide a foundation for future assessment of novel, potentially targetable pathways that alter B cell homeostasis during the diversification of B cells in the periphery when alloantigens or autoantigens are prevalent. Mouse studies can now be employed to evaluate the hierarchy of these molecules in initiating or propagating loss of B cell tolerance. The ultimate benefit of this type of single-cell level research will be the ability to design tailored therapies that eliminate or prevent the emergence of pathogenic B cells without disrupting normal humoral immune responses required for long-term health.

MATERIALS AND METHODS

Design

Single-cell RNA-Seq was performed on peripheral B cells from allo-HCT patients chosen at random, with the desire to gain new knowledge about the molecular mechanisms that emerge in the allo-HCT setting to drive B cell hyper-responsiveness and cGVHD development in some patients (loss of tolerance). Beyond some basic inclusion and exclusion criteria given to clinicians for obtaining PBMC samples for study (including cGVHD status), samples were obtained and chosen for use in a blinded fashion. For all supporting experiments, allo-HCT patient samples were likewise obtained and chosen for use in a blinded fashion.

Patient and HD blood samples

De-identified whole blood samples or apheresis samples were obtained from allo-HCT patients under IRB protocols from Duke University, the National Cancer Institute (NIH), or the Dana-Farber Cancer Institute. Informed consent was obtained from all patients, with the scope of the research and the minimal risks fully explained. Anonymous HD samples were buffy coats purchased from Gulf Coast Regional Blood Center (Houston, TX). Viably frozen PBMCs from allo-HCT patients or HDs were prepared by Ficoll-Paque® PLUS (GE Healthcare) gradient separation prior to storage in a liquid nitrogen freezer. For some experiments, purified B cells were additionally isolated immediately following PBMC gradient separation using a Human B Cell Isolation Kit II (Miltenyi Biotech), washed in cold Dulbecco's phosphate-buffered saline, and stored as B cell pellets at -80°C. The characteristics of allo-HCT patients who provided the samples used for single-cell RNA-Seq analysis and the samples used for additional experiments are described in **tables S1** and **S2,** respectively.

B cell culture, single-cell RNA-Seq library preparation, and library sequencing

B cells were purified from viably cryopreserved allo-HCT patient PBMCs using the Human B Cell Isolation Kit II (Miltenyi Biotech). B cells were then cultured for 18 h at 5% CO_2 in RPMI-1640 medium containing 10% fetal bovine serum (FBS) and 55 μM 2-Mercaptoethanol (Gibco). In some wells, cells were treated with 100 nM ATRA (MP Biomedicals, cat# 190269) for the entire culture period. The cells were then harvested, and dead cells were removed using an EasySep™ Dead Cell Removal (Annexin V) Kit (STEMCELL Technologies, Inc.). Live B cells (in HBSS containing

2% FBS) were immediately transferred on ice to the Duke Molecular Genomics Core for 10X Genomics Chromium™ Single-Cell 3' library generation according to the manufacturer's instructions and the Core Facility's standard methods, targeting 10,000 B cells per sample. 10X Genomics libraries were then transferred directly to the Duke Center for Genomic and Computational Biology, Sequencing and Genomic Technologies Shared Resource, for sequencing. All individual 10X Genomics libraries (16 total) were pooled and then applied evenly across all 4 lanes of a NovaSeq S4 Flow Cell (Illumina) with 100-bp paired-end sequencing at a depth of ~700 million reads per sample (~70,000 reads per cell).

Single-cell RNA-Seq data analysis on purified B cells from allo-HCT patients

The raw data in BCL format were de-multiplexed into FASTQs by Illumina's bcl2fastq (https://support.illumina.com). The extraction of cellular barcodes and unique molecular identifiers (UMI sequences) and genome alignment of the biological sequences were performed using the Cell Ranger pipeline (version 2.1.1, https://support.10xgenomics.com) to generate a filtered sparse matrix of gene read counts per cell. The 16 individual matrices were integrated using Stuart et al.'s method to remove batch effects (*26*). Any cells in which fewer than 500 genes were detected and those with greater than 5% mitochondrial gene counts were considered poor quality and excluded from the analysis. Any genes detected in fewer than 150 cells were likewise excluded.

Clustering analysis was conducted using R statistical environment and its extension package Seurat v3.1.4 (*26*). DEG analysis with respect to disease status (Active cGVHD vs. No cGVHD) within each cluster was performed based on the read counts across all cells within each sample using the Bioconductor package DESeq2 (version 1.26.0). Global interaction between

disease status and the B cell clusters also was analyzed. Multiple testing was accounted for within the framework of control of the false discovery rate (FDR) using the Q-value approach (version 2.14.1) (*98*). Visualizations of single-cell-level transcription profiles in UMAP space using color was performed using R package Seurat v3.1.4 (*26*). Trajectory analysis was performed to infer the relative relationship among cell clusters over 'pseudotime' using the package Slingshot (*85*).

Comparison of allo-HCT patient single-cell RNA-Seq data to a publicly available dataset on purified B cells from HDs, HIV patients, and malaria-exposed individuals

To compare scRNA data from this study to data published by Holla *et al.* (*29*), both datasets were filtered for cell quality using the same thresholds (cells with more than 5% mitochondrial gene counts, counts from fewer than 200 genes, or counts from more than 2,500 genes were excluded). High-quality cells were then filtered to retain only B cells, with cell type inferred based on signature genes from CellAssign (*99*) and expression of the union of those signature genes and the top 2000 most variable genes (following variance stabilizing transformation (*100*)) using the R package scSorter (*101*). To normalize the datasets, gene counts per cell were transformed to counts per million reads mapped (CPM) using the Seurat R package. To compare gene expression, data from the present study and *Holla et al.*(*29*) were integrated following steps recommended by the developers of Seurat. Five cohorts were integrated to account for batch effects, as follows: Holla *et al*. data (*29*) were split by sample type (HD vs. HIV vs. Malaria), and allo-HCT data was split by the two sequencing runs. To investigate biologically-relevant genes across studies and sample types, we generated a heatmap with the following attributes: We identified each subset based on a detection threshold of 50 CPM for *ITGAX* and *CD27* expression. To illustrate distribution of gene expression, values were plotted lowest to highest for each gene of interest and within each B cell

subset (*CD27*$^{+}$*ITGAX*$^{-}$, *CD27*$^{-}$*ITGAX*$^{+}$, and *CD27*$^{+}$*ITGAX*$^{+}$) and sample type. Populations with more than 100 B cells were randomly down-sampled to 100 cells. Data analyses and plot generation were carried out in the R statistical environment with packages from the comprehensive R archive network (CRAN; https://cran.r-project.org/) and the Bioconductor project (*102*). Code used to replicate the analyses and figures followed principles of reproducible analysis, leveraging knitr dynamic reports and git source code management (*103*).

Data and Code availability

All blood B cell scRNA-Seq library data from the 8 allo-HCT patients (16 samples) are available through the Gene Expression Omnibus (GEO) database (https://www.ncbi.nlm.nih.gov/geo/) under accession code GSE161343. The R scripts to reproduce the analyses of these scRNA-Seq data are available at this site: https://gitlab.oit.duke.edu/dcibioinformatics/pubs/sarantopoulos-10x-cgvhd/.

Dermal skin cell isolation and single-cell RNA-Seq analysis

A skin punch biopsy was collected from an adult allo-HCT patient with Active cGVHD in accordance with an IRB protocol approved by Duke University. Likewise, a skin punch biopsy from surgically discarded abdominoplasty tissue from a HD was obtained in accordance with an IRB protocol approved by Duke University. The skin biopsies were washed with cold DPBS and digested with 1X dispase (ThermoFisher Scientific) overnight at 4°C. The dermis was mechanically separated from the epidermis and then digested at 37°C and 5% CO2 with 0.25% trypsin/EDTA for 1.5 hr. Dermal cell suspensions were then passed through 70 µm and 40 µm cell

strainers, then pelleted by centrifugation and resuspended in Keratinocyte-SFM (ThermoFisher Scientific) containing 0.4% BSA. Single-cell suspensions were then subjected to 10X Genomics Chromium library generation and Illumina sequencing as described above. Signature gene analysis was performed using the R package Seurat to identify B cells within dermal cell clusters. DEG analysis was performed using the R package DESeq2, as described for blood B cells above. The skin cell scRNA-Seq library data will be made available through the Gene Expression Omnibus (GEO) database (https://www.ncbi.nlm.nih.gov/geo/) following peer review.

Quantitative PCR (qPCR)

Frozen (-80°C) B cell pellets were thawed on ice, and total RNA was isolated using the RNeasy Plus Mini Kit (Qiagen) and quantified with a Qubit® 3.0 Fluorometer (ThermoFisher). RNA (500 ng) was reverse-transcribed with an iScript cDNA Synthesis Kit (BioRad). *CKS2* gene expression was assessed by qPCR using *ACTB* (*β-ACTIN*) as the housekeeping gene. Primers were designed with the NCBI primer BLAST program: *CKS2*, forward 5'-ACGAGTACCGGCATGTTATGT-3' and reverse 5'-GCCTAGACTCTGTTGGACACC-3'; *ACTB*: forward, 5'-GCTGTGCTACGTCGCCCT-3' and reverse, 5'-AAGGTAGTTTCGTGGATGCC-3'. Amplification was performed using the iTaq Universal SYBR® Green Supermix (Bio-Rad) with an annealing temperature of 60°C on an ABI StepOne Plus™ Real-time PCR System (ThermoFisher Scientific). Each 20-µl reaction contained 2.5 ng of cDNA, with each primer used at a concentration of 250 nM. Data analysis was performed using Step One Software v2.3 software, and relative quantitation of gene expression was achieved using the standard-curve method. Fold change in expression in each sample was calculated using the average gene expression in patients with No cGVHD.

Flow cytometry and PhenoGraph analysis

Viably frozen PBMCs from allo-HCT patients were surface stained using antibodies against CD19, CD11c (ITGAX), CD21, CD24, CD27, EBI2 (GPR183), and TACI, along with their corresponding isotype control antibodies. 7-AAD (BioLegend) was used to assess cell viability. PhenoGraph cluster analysis was then performed on the remaining 6 markers after first pre-gating on viable B cells ($CD19^{+}$ $7AAD^{-}$), using this available function in Flowjo in combination with R. A detailed summary of all antibodies used is as follows: CD19 Pacific blue (clone J3-119, Beckman Coulter, cat#A86355); CD24 BV510 (clone ML5, BioLegend, cat#311126); CD21 FITC (Bu32, BioLegend, cat#354910); TACI PE (clone 1A1, BioLegend, cat#311906), EBI2 (GPR183) PE (clone SA313E4, BioLegend, cat#368912); CD11c APC (clone 3.9, BioLegend, cat#301614); CD27 PE-Cy7 (clone O323, eBioscience, cat#25-0279-42); IgD APC-H7 (clone IA6-2, BD Biosciences, cat#561305). Isotype control antibodies used for flow cytometry were: Mouse IgG2a BV510 (clone MOPC-173, BioLegend, cat#400268); Mouse IgG1 FITC (clone MOPC-21, BioLegend, cat#400110); Rat IgG2a PE (clone R35-95, BD Biosciences, cat#553930); Mouse IgG2a PE (clone MOPC-173, BioLegend, cat#400214); Mouse IgG1 APC (clone MOPC-21, BioLegend, cat#400120); Mouse IgG1 PE-Cy7 (clone MOPC-21, BioLegend, cat#400126); Mouse IgG2a APC-H7 (clone G155-178, BD Biosciences, cat#560897).

Phosphoarray analysis

Proteome Profiler™ Human Phospho-Kinase Array Kits (R&D Systems) were utilized according to the manufacturer's instructions to analyze whole cell lysates of purified, untreated B cell

samples from patients with Active cGVHD or No cGVHD (*n*=3 each). Spot densities on the arrays were quantified using ImageJ software (https://imagej.nih.gov/ij/).

Western blot analysis

Frozen (-80°C) pellets of purified B cells from allo-HCT patients with Active cGVHD (*n*=4) or No cGVHD (*n*=4) were lysed using a commercially available whole cell lysis buffer (Roche Complete Lysis-M) with freshly added protease inhibitors (Roche). Protein lysates were then denatured and loaded into wells of a 4–12% Bis-Tris gel (ThermoFisher) for electrophoresis under reducing conditions. Proteins were transferred from the gels to a nitrocellulose membrane using dry electroblotting (20 V for 9 min). Membranes were blocked in 2% fish gelatin buffer for 75 min and then incubated with rabbit anti-human $P27^{KIP1}$ polyclonal antibody (C-19, Santa Cruz Biotechnology, cat#sc-528, lot#KO413) overnight at 4°C. The membrane was thoroughly washed in Tris-buffered saline containing Tween 20 (TBST) before incubation for 1 h with donkey anti-rabbit polyclonal secondary antibody labeled with a near-infrared fluorescent dye (IRDye® 680, LI-COR, cat#926-68073, lot#C50821-05). The membrane was then washed thoroughly in TBST, and fluorescently labeled proteins were detected using an LI-COR Odyssey CLX Imaging System.

Supplementary Materials

Figs. S1 to S6

Tables S1 to S7

References and Notes

1. H. Wardemann *et al.*, Predominant autoantibody production by early human B cell precursors. *Science* **301**, 1374-1377 (2003).
2. H. Jin *et al.*, Antibodies from donor B cells perpetuate cutaneous chronic graft-versus-host disease in mice. *Blood*, (2016).
3. M. Srinivasan *et al.*, Donor B-cell alloantibody deposition and germinal center formation are required for the development of murine chronic GVHD and bronchiolitis obliterans. *Blood* **119**, 1570-1580 (2012).
4. R. Zeiser, S. Sarantopoulos, B. R. Blazar, B-cell targeting in chronic graft-versus-host disease. *Blood* **131**, 1399-1405 (2018).
5. A. de Masson *et al.*, CD24(hi)CD27(+) and plasmablast-like regulatory B cells in human chronic graft-versus-host disease. *Blood* **125**, 1830-1839 (2015).
6. D. Le Huu *et al.*, Donor-derived regulatory B cells are important for suppression of murine sclerodermatous chronic graft-versus-host disease. *Blood* **121**, 3274-3283 (2013).
7. J. L. Allen *et al.*, B cells from patients with chronic GVHD are activated and primed for survival via BAFF-mediated pathways. *Blood* **120**, 2529-2536 (2012).
8. W. Jia *et al.*, BAFF Promotes Heightened BCR Responsiveness and Manifestations of Chronic GVHD after Allogeneic Stem Cell Transplantation. *Blood*, (2021).
9. J. C. Poe *et al.*, An aberrant NOTCH2-BCR signaling axis in B cells from patients with chronic GVHD. *Blood* **130**, 2131-2145 (2017).
10. S. Sarantopoulos, J. Ritz, Aberrant B-cell homeostasis in chronic GVHD. *Blood* **125**, 1703-1707 (2015).

11. S. Sarantopoulos *et al.*, Altered B-cell homeostasis and excess BAFF in human chronic graft-versus-host disease. *Blood* **113**, 3865-3874 (2009).

12. A. N. Suthers, S. Sarantopoulos, TLR7/TLR9- and B Cell Receptor-Signaling Crosstalk: Promotion of Potentially Dangerous B Cells. *Front. Immunol.* **8**, 775 (2017).

13. T. Matsushita *et al.*, BAFF inhibition attenuates fibrosis in scleroderma by modulating the regulatory and effector B cell balance. *Sci Adv* **4**, eaas9944 (2018).

14. E. Zorn *et al.*, Reduced frequency of FOXP3+ CD4+CD25+ regulatory T cells in patients with chronic graft-versus-host disease. *Blood* **106**, 2903-2911 (2005).

15. E. Tivol, R. Komorowski, W. R. Drobyski, Emergent autoimmunity in graft-versus-host disease. *Blood* **105**, 4885-4891 (2005).

16. J. L. Allen *et al.*, Increased BCR responsiveness in B cells from patients with chronic GVHD. *Blood* **123**, 2108-2115 (2014).

17. R. Flynn *et al.*, Increased T follicular helper cells and germinal center B cells are required for cGVHD and bronchiolitis obliterans. *Blood* **123**, 3988-3998 (2014).

18. J. C. Poe *et al.*, SYK inhibitor entospletinib prevents ocular and skin GVHD in mice. *JCI Insight* **3**, (2018).

19. C. Zhang *et al.*, Donor CD4+ T and B cells in transplants induce chronic graft-versus-host disease with autoimmune manifestations. *Blood* **107**, 2993-3001 (2006).

20. B. R. Blazar, W. J. Murphy, M. Abedi, Advances in graft-versus-host disease biology and therapy. *Nat. Rev. Immunol.* **12**, 443-458 (2012).

21. A. Khoder *et al.*, Evidence for B Cell Exhaustion in Chronic Graft-versus-Host Disease. *Front. Immunol.* **8**, 1937 (2017).

22. X. Gao *et al.*, ZEB2 regulates the development of CD11c+ atypical B cells. *bioRxiv*, 2022.2009.2001.506173 (2022).

23. R. Yang *et al.*, Human T-bet governs the generation of a distinct subset of CD11c(high)CD21(low) B cells. *Sci Immunol* **7**, eabq3277 (2022).

24. B. Keller *et al.*, The expansion of human T-bet(high)CD21(low) B cells is T cell dependent. *Sci Immunol* **6**, eabh0891 (2021).

25. N. Obeng-Adjei *et al.*, Malaria-induced interferon-gamma drives the expansion of Tbethi atypical memory B cells. *PLoS Pathog.* **13**, e1006576 (2017).

26. T. Stuart *et al.*, Comprehensive Integration of Single-Cell Data. *Cell* **177**, 1888-1902 e1821 (2019).

27. A. Tumanov *et al.*, Distinct role of surface lymphotoxin expressed by B cells in the organization of secondary lymphoid tissues. *Immunity* **17**, 239-250 (2002).

28. E. Vigorito *et al.*, microRNA-155 regulates the generation of immunoglobulin class-switched plasma cells. *Immunity* **27**, 847-859 (2007).

29. P. Holla *et al.*, Shared transcriptional profiles of atypical B cells suggest common drivers of expansion and function in malaria, HIV, and autoimmunity. *Sci Adv* **7**, (2021).

30. H. J. Sutton *et al.*, Atypical B cells are part of an alternative lineage of B cells that participates in responses to vaccination and infection in humans. *Cell Rep.* **34**, 108684 (2021).

31. M. I. Love, W. Huber, S. Anders, Moderated estimation of fold change and dispersion for RNA-seq data with DESeq2. *Genome Biol.* **15**, 550 (2014).

32. M. Kanehisa, S. Goto, KEGG: kyoto encyclopedia of genes and genomes. *Nucleic Acids Res.* **28**, 27-30 (2000).

33. M. Ashburner *et al.*, Gene ontology: tool for the unification of biology. The Gene Ontology Consortium. *Nat. Genet.* **25**, 25-29 (2000).

34. P. E. Lipsky, Systemic lupus erythematosus: an autoimmune disease of B cell hyperactivity. *Nat. Immunol.* **2**, 764-766 (2001).

35. H. Rincon-Arevalo *et al.*, Deep Phenotyping of CD11c(+) B Cells in Systemic Autoimmunity and Controls. *Front. Immunol.* **12**, 635615 (2021).

36. A. V. Rubtsov *et al.*, CD11c-Expressing B Cells Are Located at the T Cell/B Cell Border in Spleen and Are Potent APCs. *J. Immunol.* **195**, 71-79 (2015).

37. Y. Hao, P. O'Neill, M. S. Naradikian, J. L. Scholz, M. P. Cancro, A B-cell subset uniquely responsive to innate stimuli accumulates in aged mice. *Blood* **118**, 1294-1304 (2011).

38. I. Sanz *et al.*, Challenges and Opportunities for Consistent Classification of Human B Cell and Plasma Cell Populations. *Front. Immunol.* **10**, 2458 (2019).

39. G. J. Brown *et al.*, TLR7 gain-of-function genetic variation causes human lupus. *Nature* **605**, 349-356 (2022).

40. S. A. Jenks, K. S. Cashman, M. C. Woodruff, F. E. Lee, I. Sanz, Extrafollicular responses in humans and SLE. *Immunol. Rev.* **288**, 136-148 (2019).

41. S. A. Jenks *et al.*, Distinct Effector B Cells Induced by Unregulated Toll-like Receptor 7 Contribute to Pathogenic Responses in Systemic Lupus Erythematosus. *Immunity* **49**, 725-739 e726 (2018).

42. H. T. Greinix *et al.*, Elevated numbers of immature/transitional CD21- B lymphocytes and deficiency of memory CD27+ B cells identify patients with active chronic graft-versus-host disease. *Biol. Blood Marrow Transplant.* **14**, 208-219 (2008).

43. I. Isnardi *et al.*, Complement receptor 2/CD21- human naive B cells contain mostly autoreactive unresponsive clones. *Blood* **115**, 5026-5036.

44. S. Moir, A. S. Fauci, B-cell exhaustion in HIV infection: the role of immune activation. *Curr. Opin. HIV AIDS* **9**, 472-477 (2014).

45. Y. Li, Z. Li, F. Hu, Double-negative (DN) B cells: an under-recognized effector memory B cell subset in autoimmunity. *Clin. Exp. Immunol.* **205**, 119-127 (2021).

46. C. Wei *et al.*, A new population of cells lacking expression of CD27 represents a notable component of the B cell memory compartment in systemic lupus erythematosus. *J. Immunol.* **178**, 6624-6633 (2007).

47. E. Masle-Farquhar *et al.*, Uncontrolled CD21(low) age-associated and B1 B cell accumulation caused by failure of an EGR2/3 tolerance checkpoint. *Cell Rep.* **38**, 110259 (2022).

48. J. Brummelman *et al.*, Development, application and computational analysis of high-dimensional fluorescent antibody panels for single-cell flow cytometry. *Nat. Protoc.* **14**, 1946-1969 (2019).

49. X. Liu *et al.*, A comparison framework and guideline of clustering methods for mass cytometry data. *Genome Biol.* **20**, 297 (2019).

50. F. Corrente *et al.*, CD21(-) CD27(-) Atypical B Cells in a Pediatric Cohort Study: An Extensive Single Center Flow Cytometric Analysis. *Front Pediatr* **10**, 822400 (2022).

51. A. Arazi *et al.*, The immune cell landscape in kidneys of patients with lupus nephritis. *Nat. Immunol.* **20**, 902-914 (2019).

52. D. R. Glass *et al.*, An Integrated Multi-omic Single-Cell Atlas of Human B Cell Identity. *Immunity* **53**, 217-232 e215 (2020).

53. D. Nehar-Belaid *et al.*, Mapping systemic lupus erythematosus heterogeneity at the single-cell level. *Nat. Immunol.* **21**, 1094-1106 (2020).

54. F. Zhang *et al.*, Defining inflammatory cell states in rheumatoid arthritis joint synovial tissues by integrating single-cell transcriptomics and mass cytometry. *Nat. Immunol.* **20**, 928-942 (2019).

55. A. V. Sauer *et al.*, Defective B cell tolerance in adenosine deaminase deficiency is corrected by gene therapy. *J. Clin. Invest.* **122**, 2141-2152 (2012).

56. C. Schaniel *et al.*, Activated murine B lymphocytes and dendritic cells produce a novel CC chemokine which acts selectively on activated T cells. *J. Exp. Med.* **188**, 451-463 (1998).

57. M. L. Allende *et al.*, S1P1 receptor directs the release of immature B cells from bone marrow into blood. *J. Exp. Med.* **207**, 1113-1124 (2010).

58. T. I. Arnon, R. M. Horton, I. L. Grigorova, J. G. Cyster, Visualization of splenic marginal zone B-cell shuttling and follicular B-cell egress. *Nature* **493**, 684-688 (2013).

59. J. A. Green *et al.*, The sphingosine 1-phosphate receptor S1P(2) maintains the homeostasis of germinal center B cells and promotes niche confinement. *Nat. Immunol.* **12**, 672-680 (2011).

60. I. Y. Hwang, C. Park, K. Harrison, J. H. Kehrl, Biased S1PR1 Signaling in B Cells Subverts Responses to Homeostatic Chemokines, Severely Disorganizing Lymphoid Organ Architecture. *J. Immunol.* **203**, 2401-2414 (2019).

61. G. Muller, M. Lipp, Shaping up adaptive immunity: the impact of CCR7 and CXCR5 on lymphocyte trafficking. *Microcirculation* **10**, 325-334 (2003).

62. G. Nunez, D. Hockenbery, T. J. McDonnell, C. M. Sorensen, S. J. Korsmeyer, Bcl-2 maintains B cell memory. *Nature* **353**, 71-73 (1991).

63. A. Kieser, Pursuing different 'TRADDes': TRADD signaling induced by TNF-receptor 1 and the Epstein-Barr virus oncoprotein LMP1. *Biol. Chem.* **389**, 1261-1271 (2008).

64. K. Inada *et al.*, c-Fos induces apoptosis in germinal center B cells. *J. Immunol.* **161**, 3853-3861 (1998).

65. M. Mandal *et al.*, CXCR4 signaling directs Igk recombination and the molecular mechanisms of late B lymphopoiesis. *Nat. Immunol.* **20**, 1393-1403 (2019).

66. D. Gatto, D. Paus, A. Basten, C. R. Mackay, R. Brink, Guidance of B cells by the orphan G protein-coupled receptor EBI2 shapes humoral immune responses. *Immunity* **31**, 259-269 (2009).

67. A. E. Hauser *et al.*, Chemotactic responsiveness toward ligands for CXCR3 and CXCR4 is regulated on plasma blasts during the time course of a memory immune response. *J. Immunol.* **169**, 1277-1282 (2002).

68. J. R. Muppidi, E. Lu, J. G. Cyster, The G protein-coupled receptor P2RY8 and follicular dendritic cells promote germinal center confinement of B cells, whereas S1PR3 can contribute to their dissemination. *J. Exp. Med.* **212**, 2213-2222 (2015).

69. J. P. Pereira, L. M. Kelly, Y. Xu, J. G. Cyster, EBI2 mediates B cell segregation between the outer and centre follicle. *Nature* **460**, 1122-1126 (2009).

70. E. Lu, F. D. Wolfreys, J. R. Muppidi, Y. Xu, J. G. Cyster, S-Geranylgeranyl-L-glutathione is a ligand for human B cell-confinement receptor P2RY8. *Nature* **567**, 244-248 (2019).

71. Y. He *et al.*, P2RY8 variants in lupus patients uncover a role for the receptor in immunological tolerance. *J. Exp. Med.* **219**, (2022).

72. R. Deng *et al.*, Extrafollicular CD4(+) T-B interactions are sufficient for inducing autoimmune-like chronic graft-versus-host disease. *Nat Commun* **8**, 978 (2017).

73. D. E. Kennedy *et al.*, Novel specialized cell state and spatial compartments within the germinal center. *Nat. Immunol.* **21**, 660-670 (2020).

74. G. Koncz, A. O. Hueber, The Fas/CD95 Receptor Regulates the Death of Autoreactive B Cells and the Selection of Antigen-Specific B Cells. *Front. Immunol.* **3**, 207 (2012).

75. J. K. Lee, S. O. Mathew, S. V. Vaidya, P. R. Kumaresan, P. A. Mathew, CS1 (CRACC, CD319) induces proliferation and autocrine cytokine expression on human B lymphocytes. *J. Immunol.* **179**, 4672-4678 (2007).

76. S. Sarantopoulos *et al.*, High levels of B-cell activating factor in patients with active chronic graft-versus-host disease. *Clin. Cancer Res.* **13**, 6107-6114 (2007).

77. Y. Saito *et al.*, B-cell-activating factor inhibits CD20-mediated and B-cell receptor-mediated apoptosis in human B cells. *Immunology* **125**, 570-590 (2008).

78. S. Chevrier *et al.*, The BTB-ZF transcription factor Zbtb20 is driven by Irf4 to promote plasma cell differentiation and longevity. *J. Exp. Med.* **211**, 827-840 (2014).

79. S. Minguet *et al.*, Caveolin-1-dependent nanoscale organization of the BCR regulates B cell tolerance. *Nat. Immunol.* **18**, 1150-1159 (2017).

80. N. Bhat *et al.*, Regnase-1 is essential for B cell homeostasis to prevent immunopathology. *J. Exp. Med.* **218**, (2021).

81. D. J. Hodson *et al.*, Regulation of normal B-cell differentiation and malignant B-cell survival by OCT2. *Proc. Natl. Acad. Sci. U. S. A.* **113**, E2039-2046 (2016).

82. G. Pearce *et al.*, Signaling protein SWAP-70 is required for efficient B cell homing to lymphoid organs. *Nat. Immunol.* **7**, 827-834 (2006).

83. G. Pearce, T. Audzevich, R. Jessberger, SYK regulates B-cell migration by phosphorylation of the F-actin interacting protein SWAP-70. *Blood* **117**, 1574-1584 (2011).

84. M. Yang *et al.*, AIM2 deficiency in B cells ameliorates systemic lupus erythematosus by regulating Blimp-1-Bcl-6 axis-mediated B-cell differentiation. *Signal Transduct Target Ther* **6**, 341 (2021).

85. K. Street *et al.*, Slingshot: cell lineage and pseudotime inference for single-cell transcriptomics. *BMC Genomics* **19**, 477 (2018).

86. F. C. Guibal *et al.*, ASB-2 inhibits growth and promotes commitment in myeloid leukemia cells. *J. Biol. Chem.* **277**, 218-224 (2002).

87. H. E. Parge, A. S. Arvai, D. J. Murtari, S. I. Reed, J. A. Tainer, Human CksHs2 atomic structure: a role for its hexameric assembly in cell cycle control. *Science* **262**, 387-395 (1993).

88. M. Frontini *et al.*, The CDK subunit CKS2 counteracts CKS1 to control cyclin A/CDK2 activity in maintaining replicative fidelity and neurodevelopment. *Dev. Cell* **23**, 356-370 (2012).

89. K. Hiromura, J. W. Pippin, M. L. Fero, J. M. Roberts, S. J. Shankland, Modulation of apoptosis by the cyclin-dependent kinase inhibitor p27(Kip1). *J. Clin. Invest.* **103**, 597-604 (1999).

90. M. D. Larrea *et al.*, RSK1 drives p27Kip1 phosphorylation at T198 to promote RhoA inhibition and increase cell motility. *Proc. Natl. Acad. Sci. U. S. A.* **106**, 9268-9273 (2009).

91. J. D. Short *et al.*, AMPK-mediated phosphorylation of murine p27 at T197 promotes binding of 14-3-3 proteins and increases p27 stability. *Mol. Carcinog.* **49**, 429-439 (2010).

92. A. V. Rubtsov *et al.*, Toll-like receptor 7 (TLR7)-driven accumulation of a novel CD11c(+) B-cell population is important for the development of autoimmunity. *Blood* **118**, 1305-1315 (2011).

93. C. D. Scharer *et al.*, Epigenetic programming underpins B cell dysfunction in human SLE. *Nat. Immunol.* **20**, 1071-1082 (2019).

94. S. Wang *et al.*, IL-21 drives expansion and plasma cell differentiation of autoreactive CD11c(hi)T-bet(+) B cells in SLE. *Nat Commun* **9**, 1758 (2018).

95. E. Zumaquero *et al.*, IFNgamma induces epigenetic programming of human T-bet(hi) B cells and promotes TLR7/8 and IL-21 induced differentiation. *Elife* **8**, (2019).

96. S. Sarantopoulos *et al.*, Recovery of B-cell homeostasis after rituximab in chronic graft-versus-host disease. *Blood* **117**, 2275-2283 (2011).

97. N. F. Smirnova *et al.*, Inhibition of B cell-dependent lymphoid follicle formation prevents lymphocytic bronchiolitis after lung transplantation. *JCI Insight* **4**, (2019).

98. J. Bass, A. Swcf, A. Dabney, D. Robinson, qvalue: Q-value estimation for false discovery rate control. *R package version 2.8.0, http://github.com/jdstorey/qvalue*, (2015).

99. A. W. Zhang *et al.*, Probabilistic cell-type assignment of single-cell RNA-seq for tumor microenvironment profiling. *Nat Methods* **16**, 1007-1015 (2019).

100. S. Anders, W. Huber, Differential expression analysis for sequence count data. *Genome Biol.* **11**, R106 (2010).

101. H. Guo, J. Li, scSorter: assigning cells to known cell types according to marker genes. *Genome Biol.* **22**, 69 (2021).

102. R. C. Gentleman *et al.*, Bioconductor: open software development for computational biology and bioinformatics. *Genome Biol.* **5**, R80 (2004).

103. K. Ram, Git can facilitate greater reproducibility and increased transparency in science. *Source Code Biol. Med.* **8**, 7 (2013).

Acknowledgments:

The authors wish to thank Laney Weber, Certified Editor in the Life Sciences, for the critical review of this manuscript and assistance with formatting. The authors also wish to thank Lauren S. Riley and Serach Patterson for assistance with proofreading.

Funding:

National Institutes of Health (NHLBI) grant R01HL129061 (SS)

Leukemia & Lymphoma Society grant 6497-16 (SS)

National Institutes of Health (NIAID) grant R38AI140297 (SJB)

European Union's Horizon 2020 Research and Innovation Program under the Marie Sklodowska-Curie grant agreement No 888743 (JV, SS)

Author contributions:

Conceptualization: JCP, SS

Data curation: JF, MRL, KO

Formal analysis: JF, DZ, MRL, XQ, JX, KO

Funding acquisition: SS, SJB, JV

Investigation: JCP, RAD, HS, JZ, ANS, ICC

Methodology: JF, DZ, MRL, RAD, XQ, JV, JX, KO

Resources: VTH, KSW, JJR, SZP, FTH, MEH, DAR, ARC

Software: JF, DZ, MRL, XQ, JX, KO

Supervision: SS, KO

Validation: JF, MRL, XQ, KO

Visualization: JCP, JF, JV, KO, SS

Writing – original draft: JCP, SS, KO

Writing – review & editing: JF, DZ, MRL, RAD, XQ, JZ, JV, SJB, WJ, WM, NJC, ARC, JX

Competing interests: The authors report no conflict of interest related to this study.